

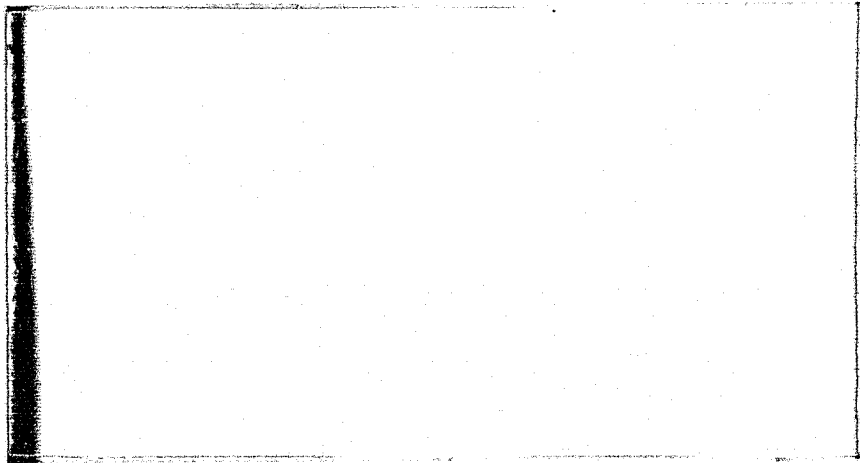
General Disclaimer

One or more of the Following Statements may affect this Document

- This document has been reproduced from the best copy furnished by the organizational source. It is being released in the interest of making available as much information as possible.
- This document may contain data, which exceeds the sheet parameters. It was furnished in this condition by the organizational source and is the best copy available.
- This document may contain tone-on-tone or color graphs, charts and/or pictures, which have been reproduced in black and white.
- This document is paginated as submitted by the original source.
- Portions of this document are not fully legible due to the historical nature of some of the material. However, it is the best reproduction available from the original submission.

NASW-184

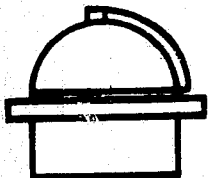
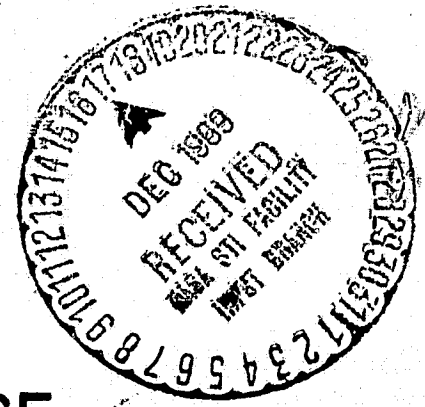
SOLAR SATELLITE PROJECT



N70-20438 <small>(ACCESSION NUMBER)</small>	 <small>(THRU)</small>
37 <small>(PAGES)</small>	30 <small>(CODE)</small>
0-108916 <small>(NASA CR OR TMX OR AD NUMBER)</small>	 <small>(CATEGORY)</small>

FACILITY FORM 802

DRE



HARVARD COLLEGE OBSERVATORY

60 GARDEN STREET
CAMBRIDGE, MASS

SOLAR XUV LIMB BRIGHTENING
OBSERVATIONS AND INTERPRETATION

Technical Report #13

George L. Withbroe

November, 1969

Harvard College Observatory

PART I

THE LITHIUM-LIKE IONS

1. Introduction and Observations

This paper describes results of an analysis of equatorial solar-limb brightening for resonance lines of the lithium-like ions N V, O VI, Ne VIII, Mg X, and Si XII. An important characteristic of these lines is that they can be observed both on the disk and above the limb. This feature and the fact that the ions are formed at temperatures ranging from $2 \cdot 10^5$ °K. to $2 \cdot 10^6$ °K makes them very useful for studying models of the chromospheric-coronal transition region and lower corona.

The observations were obtained with the Harvard spectrometer-spectroheliometer on OSO-IV in November 1967 (Goldberg et al., 1968). In the spectroheliographic mode of operation spectroheliograms were obtained every five minutes. The individual spectroheliograms consist of a 40 x 48 matrix of data points which correspond to a 36 arc minute square area. The spatial resolution of the measurements is one arc minute. During the hour of daylight in each orbit, 10 to 12 spectroheliograms were made at one wavelength. The wavelength being monitored was usually changed once per orbit or every 90 - 100 minutes. Usually several spectroheliograms from an orbit were of inferior quality because

of the effects of atmospheric absorption, noise caused by passage through the south Atlantic geomagnetic anomaly, or because the spectrometer wavelength was being changed.

To construct limb-brightening curves for the solar equatorial belt, data from 5 to 7 orbits were used for each spectral line. The orbits chosen for study were sufficiently far apart in time, several days to several weeks, that solar rotation would tend to smooth out the effects of coronal structure in the equatorial region. Only data between solar latitudes $+10^\circ$ and -10° were used. This latitude range avoids most active regions and gives sufficient data for the construction of smooth limb-brightening curves. For each orbit a mean spectroheliogram was obtained by averaging data from the 6-8 best spectroheliograms in the orbit. These averaged data points were then plotted by a computer-driven plotter. Typical limb brightening data are shown for the O VI line at 1032 \AA in Figure 1. The ordinate is proportional to the logarithm of the mean intensity in a one arc minute square region on the solar disk. The abscissa is the distance from the center of the solar disk in units defined by the north-south spacing of the data points in the spectroheliograms. The solar limb is at a distance of 21.3 of these units.

The vertical scatter of the points is caused primarily by coronal inhomogeneities whose sizes are equal to or larger than the spatial resolution of the instrument. The points farthest from the mean curve are those obtained from the edges of active regions that penetrate into the equatorial belt. A small portion of the scatter is caused by statistical fluctuations in the pulses counted by the photoelectric detection system. Since each intensity value represents the average of approximately 6 independent measurements of a signal with a mean value of 600 counts per integration period, the statistical noise is the order of $\sqrt{600}/\sqrt{6} = 10$ counts. This value is about 2% of the mean, while the root-mean-square fluctuation of the intensity across the surface of the sun is 23% of the mean. For Mg X the rms fluctuations are somewhat higher, 40% of the mean intensity in the line. Since the intensities of UV lines are proportional to the square of the electron density, this means that the minimum rms fluctuation of the electron density in the equatorial corona is the order of 10 to 20%.

From data such as those presented in Figure 1, mean limb-brightening curves have been generated for a number of lines, in particular, the resonance lines $\lambda 1239$ of N V, $\lambda 1032$ of O VI, $\lambda 770$ of Ne VIII, $\lambda 625$ of Mg X, and $\lambda 499$ of Si XII. Each of

these lines is one of the two lines of the first multiplet ($1s^2 2s^2 S_{1/2} - 1s^2 2p^2 P_{1/2,3/2}$) of a lithium-like ion. In most cases the other line of the multiplet is blended with a first or second order line of a different atomic species.

The absolute scale of the observations was determined by comparing OSO-IV data with published and unpublished solar UV flux measurements made by Hall, Hinteregger, and their coworkers. We are indebted to them for supplying their data in advance of publication. Only chromospheric spectral features were used in the comparison. We had hoped to supply our own independent absolute flux and intensity measurements, but the sensitivity of the OSO-IV experiment changed substantially in orbit. Since important changes in sensitivity appear to have occurred before the instrument was turned on one week after launch, the pre-flight laboratory calibration performed on the instrument could not be used to place the OSO-IV observations on an absolute scale. A complete description of the entire calibration problem will be published by Reeves et al. at a later date. The OSO-IV absolute intensities should be accurate to within a factor of 3.

2. Coronal Model

From an analysis of rocket measurements of solar fluxes emitted by XUV spectral lines, Athay (1966) derived a model for the chromospheric-coronal transition region and lower corona. His study shows that over a fairly wide range of temperatures, the energy conducted from the corona to the chromosphere under conditions of constant conductive flux appears to control the temperature structure of the corona. The expected form of the temperature gradient under these conditions (Chapman, 1954) is

$$\frac{dT}{dh} = \frac{1}{c} T_e^{-5/2}$$

Athay used calculations of the ionization equilibrium which did not include the effects of dielectronic recombination. A later study by Dupree and Goldberg (1967) shows that inclusion of these effects does not change the essential features of Athay's results. In Dupree and Goldberg's model the temperature gradient varies as $T_e^{-5/2}$ over the range $10^5 \leq T_e \leq 10^{6.2}$ °K.

The XUV data used by Athay and by Dupree and Goldberg are measurements of the energy radiated by the entire solar atmosphere. Their coronal models assume that this radiation comes from a corona that is homogeneous and spherically symmetric. The presence of active regions on the disk and

polar darkening observed in some XUV lines (cf. Goldberg et al. 1968) raises the question as to which areas the models best represent. This depends upon the relative contribution to the total solar flux of the quiet areas, polar areas, and active regions. An examination of OSO-IV data shows that for XUV lines formed at temperatures less than about 10^6 °K, the flux radiated by the entire solar disk is characteristic of the equatorial quiet area. For this reason the coronal model of Athay and the model of Dupree and Goldberg represent conditions in the equatorial corona, at least for the layers in which the temperature gradient appears to vary as $T_e^{-5/2}$. In a future paper we shall discuss differences in the XUV radiation emitted by quiet and active regions.

In their calculations Dupree and Goldberg assumed that the scaled electron pressure $P_e = n_e T_e$ is constant over the entire chromospheric-coronal transition region and has a value of $6 \cdot 10^{14}$. This is a fairly good approximation for the temperature range $4.7 \leq \log T_e \leq 6$ K, because the geometrical thickness of the transition region is small compared to the pressure scale height. Although the assumption of constant electron pressure is useful for the interpretation of UV flux data, it has limitations in the interpretation of intensity data which

include observations made at one or two pressure scale heights above the limb. Therefore, for the initial interpretation of the OSO-IV limb-brightening data, we have adopted the model to be described: The dependence of electron temperature on height in a transition region, for $\log T_e \leq 6.3$, is the same as determined by Dupree and Goldberg (Fig. 2). To this transition region we have attached a corona with a constant temperature of 2 million degrees. Ground based observations of the corona suggest that the coronal temperature is between 1.5 and 2.0 million degrees K (cf. Billings, 1966; Newkirk, 1967; Zirin, 1966). A value of 2 million degrees was used because the presence of Si XII emission in quiet areas of the solar disk indicates that a substantial portion of the quiet corona is near this temperature. This point will be discussed in greater detail in Section 4. For the electron pressure in the transition region at the height where $T_e = 10^5$, we have adopted the same value used by Dupree and Goldberg. The electron densities and pressures at other heights were computed from formulae consistent with the assumption of hydrostatic equilibrium. The resulting model is equivalent to that of Dupree and Goldberg for the range $5 \leq \log T_e \leq 6$, but departs

from their model for temperatures greater than 10^6 K, because the electron pressure decreases with increasing height above this level.

The adopted model predicts a brightness for the white light K-corona that agrees reasonably well with HAO measurements made at 2 arc minutes above the limb during November 1967. We are indebted to Dr. R. Hansen for sending us K-coronometer data prior to publication. The observed parameter is pb where p is the polarization and b is the brightness in units of 10^{-8} of the brightness of the solar disk. The observed value of pb during November 1967 in the equatorial corona is approximately 55 while in the adopted model the value is 46. The quantity pb for the model was calculated from the formulae given by van de Hulst (1950).

3. Theory

Let us assume that the coronal lines are produced in two-level atoms with frequency-independent source functions. The source function (Avrett and Hummer, 1965) can be written as

$$S(\tau_0) = (1-\epsilon) \cdot \int_{-\infty}^{\infty} \Phi_x J_x(\tau_0) dx + \epsilon B(\tau_0) \quad (1)$$

where τ_0 is the optical depth at line center, B is the Planck function determined from the electron temperature at τ_0 , and J_x is the mean intensity in the line. The line broadening is given by the normalized Doppler expression

$$\Phi_x = \frac{1}{\sqrt{\pi}} e^{-x^2} \quad (2)$$

where $x = \Delta\nu/\Delta\nu_0$, $\Delta\nu_0$ is the Doppler width, and

$$\epsilon B = \frac{C_{21}}{A_{21}} \left(1 - e^{-h\nu/kT} \right) \quad (3)$$

The quantity C_{21} is the collisional transition rate from level 2 to 1, A_{21} is the radiative transition rate, and for coronal lines $A_{21} \gg C_{21}$. The optical depths, τ_0 , of the lines considered here are small, of the order of 0.1 or smaller when computed with the Dupree and Goldberg model. This means that the first term on the right side of equation (1) is small compared to ϵB . We assume as a first approximation that

$$S(\tau_0) = K \cdot \epsilon B \quad (4)$$

Use of this expression eliminates the need to solve the transfer equation and gives intensities which are accurate to within about 10% or better for the lines used in this analysis. This was determined by solving the transfer equation with an

iterative method. The method used to determine K is given at the end of this section.

The emergent intensity at a distance ρ from the center of the solar disk is

$$I_x(\rho) = \int_{-\infty}^{\tau_x} S(t_x) e^{-t_x/\mu} dt_x/\mu \quad (5)$$

where τ_x is the optical thickness of the line-forming region at frequency x , t_x is the optical depth at frequency x , ρ is the distance in units of R_\odot from the center of the sun to the line-of-sight at the point where the line-of-sight is closest to the center of the sun, $\mu = \sqrt{r^2 - (\rho R_\odot)^2}/r$ for $\rho < 1$ and μ is one half this quantity for $\rho \geq 1$, r is the distance from the center of the sun, and R_\odot is the radius of the sun.

If we assume that the Doppler width is constant over the region of line formation, equation (5) can be rewritten as

$$I_x(\rho) = \int_{-\infty}^{\tau} S(t) \cdot e^{-\Phi_x t/\mu} \Phi_x dt/\mu \quad (6)$$

where $t = t_x/\Phi_x$. The observed quantity is the the total intensity in the line:

$$I(\rho) = \Delta\nu_0 \int_{-\infty}^{\infty} I_x(\rho) dx = \Delta\nu_0 \int_{-\infty}^{\infty} \int_{-\infty}^{\tau} S(t) e^{-\Phi_x t/\mu} \Phi_x dt/\mu dx \quad (7)$$

$$= \Delta\nu_0 \int_{-\infty}^{\tau} S(t) \Phi(t/\mu) dt/\mu \quad (8)$$

where

$$\Phi(t/\mu) = \int_{-\infty}^{\infty} \Phi_x e^{-\Phi_x t/\mu} dx .$$

From Seaton (1964) we have

$$C_{12} = 1.7 \cdot 10^{-3} \cdot g \cdot n_e \cdot T_e^{-1/2} \cdot w^{-1} \cdot f \cdot 10^{(-5040 w/T_e)} . \quad (10)$$

By definition

$$C_{21} = C_{12} e^{hv/kT} \frac{\tilde{w}_1}{\tilde{w}_2} , \quad (11)$$

$$A_{21} = \frac{\tilde{w}_1}{\tilde{w}_2} 8\pi^2 \frac{e^2 v^2}{mc^3} f , \quad (12)$$

where f is the oscillator strength of the line, g is the mean Gaunt factor, W is the excitation energy in electron volts, \tilde{w}_1 and \tilde{w}_2 are statistical weights, and other quantities have their usual definitions.

Since the great majority of the atoms are in the ground state, level 1, we have

$$\begin{aligned} dt &= n_1 \alpha_0 dh / \Phi_0 \\ &= n_1 \frac{\sqrt{\pi} e^2}{mc} \cdot \frac{f}{\Delta\nu_0} dh / \Phi_0 , \end{aligned} \quad (13)$$

From equations (8) - (13) one obtains

$$I(\rho) = 3.77 \cdot 10^{-21} \cdot A \cdot g \cdot f \cdot K \int_0^{\infty} G(T_e) \Phi(t/\mu) n_e^2 dh/\mu \quad (14)$$

where

$$G(T_e) = R_i(T_e) \cdot T_e^{-1/2} \cdot 10^{(-5040 \cdot w/T_e)} \quad (15)$$

From $\rho > 1$ the lower limit on the integral is $h_0 = (\rho - 1) R_\odot$. This formula makes use of the fact that most ions are in the ground state and therefore that

$$n_1 = n_i = \frac{n_i}{n_a} \frac{n_a}{n_H} \frac{n_H}{n_e} n_e = 0.8 n_e \cdot R_i \cdot A \quad (16)$$

where n_i (cm^{-3}) is the number of ions of the type producing the line, n_a (cm^{-3}) is the total number of atoms summed over all stages of ionization of the element, n_H (cm^{-3}) is the number of neutral and ionized hydrogen atoms, n_e (cm^{-3}) is the number of electrons, $n_H = 0.8 n_e$ for a fully ionized gas with $N_{\text{He}}/N_H = 0.1$, $R_i = n_i/n_a$, and $A = n_a/n_H$ is the abundance of the element. The quantity R_i is a function of temperature. We have used values of R_i computed by Allen and Dupree (1969) and some unpublished values computed with the same technique by Wood and Dupree (1969). These calculations included the effects of dielectronic recombination and autoionization processes.

Since all photons created by collisional excitations from level 1 to 2 and radiative transitions from 2 to 1 escape the line forming region (Athay, 1966), the emergent flux from the

sun is

$$F = 1/2 h\nu \int_0^{\infty} n_1 c_{12} dh \quad (17)$$

By using a procedure similar to that used in developing equation (14) one can show that

$$F = 1/2 h\nu K \int_0^{\infty} n_1 c_{12} K_2(t) dh \quad (18)$$

where

$$K_2(t) = \int_{-\infty}^{\infty} \Phi_x E_2(\Phi_x \cdot t) dx \quad (19)$$

and E_2 is the second exponential integral. From equations (17) and (18) we obtain

$$K = \frac{\int_0^{\infty} n_1 c_{12} dh}{\int_0^{\infty} n_1 c_{12} K_2(t) dh} \quad (20)$$

The f-values and Gaunt factors used in the analysis are given in Table 1. Also given is the temperature at which the function $G(T_e)$ (eq. 15) has its maximum value. This temperature provides an indication as to where formation of the ion is most strongly favored.

4. Results

The modified Dupree and Goldberg model described in Section 2 predicts that the limb brightening of the lines N V λ 1239, O VI λ 1032, Ne VII λ 770, Mg X λ 625 and Si XII λ 499 should have the form given in Figure 3. The ion with the lowest ionization potential, N V, is formed almost entirely in the narrow transition region. As the ionization potential of the ion increases, the corona contributes more and more to the emergent intensity of the line, raising the intensity above the limb ($\rho > 1$) with respect to the intensity on the disk ($\rho < 1$).

The limb brightening curves obtained from the OSO-IV spectroheliograms agree remarkably well with predicted curves, as shown in Figures 4-8. The figures give intensities in terms of the mean intensity at the center of the disk, $I(0)$. Values for $I(0)$ are given in Table 1. The solid line represents the limb brightening predicted with the modified Dupree and Goldberg model after the curves have been smoothed with the one arc minute aperture function of the OSO-IV instrument. The dashed lines in Figures 4-6 represent the instrumental limb profile for a spectral line with no corona component. This is an empirical profile determined from spectroheliograms in a number of lines arising from atoms in low stages of ionization such as He I, C II, O I, H I, etc. The dotted line is the

predicted limb brightening for $\rho > 1$ including the effects of empirical limb profile.

Two sets of points are given for the N V line (Fig. 4). The N V line is blended with the wing of hydrogen Lyman α and several atomic continua, which together form a quasi-continuum with an intensity equal to that of the N V line. This continuum was subtracted from the $\lambda 1239$ spectroheliograms with the aid of two assumptions: (1) that the continuum has a $1/\mu$ behavior (circles) and (2) that the continuum does not vary from center to limb (crosses). The first of these assumptions appears to give a better fit to the theoretical curve. The intensity of the continuum at the center of the solar disk was determined from OSO-IV spectral scans. The N V line was observed for only one orbit, so that its limb brightening may be more affected by structures in the equatorial region than are the other lines where limb brightening curves were derived from data averaged over 6 or 7 orbits widely spaced in time. The intensity beyond the limb for N V is very close to the level of the instrumentally scattered light (dashed line). For this reason it is not possible to determine reliable N V intensities for $\rho > 1$; however, upper limits can be defined.

For the Ne VIII line at 770Å and Si XII line at 499Å, it was necessary to subtract, respectively, the underlying hydrogen Lyman continuum and the helium continuum. This was done through use of observations of limb brightening at nearby wavelengths in these continua and XUV spectra of the center of the quiet disk. For example, observations were made at a number of wavelengths in the Lyman continuum including substantial data at 800Å. Spectra of the center of the solar disk were used to determine the ratio of the intensity of the Lyman continuum at 770Å and 800Å. With this ratio and the observed center-to-limb variation of the intensity at 800Å, it was possible to determine as a function of limb position the contribution of the Lyman continuum to the total intensity observed at 770Å. The Lyman continuum at 770Å amounts to 40% of the intensity of the Ne VIII line in the central portion of the disk. The He I intensity at 499Å averaged over the central portion of the disk is slightly larger than the mean intensity in the Si XII line.

While the agreement between the predicted and observed limb brightening for the lines studied is fairly good, there appear to be some systematic differences. The theoretical curves have been forced to fit the observations best for $\rho < 1$. This results in some systematic differences between the theoretical and observed intensities for $\rho > 1$. We shall show below how small changes in the parameters describing

the coronal model can account for these differences.

Note that in Dupree and Goldberg's model the coronal abundances of O and Si are equal to their photospheric values. In order to obtain a good fit between the observed and computed limb-brightening curves, it was necessary to use somewhat different abundances, which are shown in Table 2. Although the modified Dupree and Goldberg model predicts the shape of the limb-brightening curves remarkably well, it gives absolute intensities which tend to be too small, by about a factor of 3, if photospheric abundances are used in the calculations.

What are the implications of these results? The important characteristic of the modified Dupree and Goldberg model is that for $T_e \gtrsim 10^5$ the model is completely specified by three parameters, C , T_c , and P_e . The model consists of a transition region where

$$\left(\frac{dT}{dh}\right)^{-1} = C \cdot T^{5/2}, \quad (21)$$

to which is attached a corona with a temperature equal to T_c . The density is determined by fixing the value of the electron pressure P_e in the transition region at the level where $\log T_e = 5$ and using formulae consistent with the assumption of hydrostatic equilibrium.

How sensitive are the XUV limb-brightening curves to the assumed values of these parameters? The ratio of the intensity for $\rho > 1$ to the intensities for $\rho < 1$ is very sensitive to the assumed values of C and T_c for the lines of N V, Ne VIII, and O VI. This is shown in Figures 9 and 10 for O VI. In Figure 9 T_c has been fixed at a value of 2 million degrees K while $\log C$ is varied over the range -11.7 to -12.3. In Figure 10 $\log C$ has been fixed at -12.0, while $\log T_c$ is varied over the range 6.2 to 6.4 ($1.6 \cdot 10^6 \leq T_c \leq 2.5 \cdot 10^6$). These results suggest that if we can determine T_c , the value of C can then be found from curves such as those in Figure 10.

The value of T_c can be fixed by using observations above the limb, $\rho > 1$. Since the optical depths in the lines are small, we obtain from equation (14)

$$\frac{I(\text{Si XII})}{I(\text{O VI})} = \frac{A_{\text{Si}}}{A_{\text{O}}} \frac{[gf G(T_c)]_{\text{Si XII}}}{[gf G(T_c)]_{\text{O VI}}}$$

etc. The intensity ratios Si XII/N V, Si XII/O VI, Si XII/Ne VIII, Si XII/Mg X, are very sensitive to temperature. Figure 11 shows the predicted ratios as a function of temperature when photospheric abundances are used. The circles plotted on the curves are

the observed ratios for coronal layers above the limb, $\rho > 1.08$. The observed ratio for Si XII/N V is a lower limit because of uncertainty in the contribution of scattered light to the N V intensity for $\rho > 1$. Some analyses of UV flux measurements (Athay, 1966; Dupree and Goldberg, 1967) indicate that observations of UV lines can be explained by use of photospheric abundances. Other analyses (Jordan, 1966; Pottasch, 1967) suggest that coronal abundances differ significantly from the photospheric values. For this reason we have included in Figure 11 the temperatures that result when the observed intensity ratios are plotted on curves generated with Pottasch's abundances (squares) and Athay's abundances (triangles). The coronal temperature $2 \cdot 10^6$ °K appears to be the most consistent with the OSO observations and previous abundance determinations. It should be noted that relative intensities of the different lines are accurate to only about a factor of 2. Since there are also uncertainties in the relative coronal abundances of the chemical elements, our value for T_c is probably accurate to about 30%.

Once the coronal temperature T_c has been determined, it is a simple task to find the constant C in equation (19). The values obtained from the O VI and Ne VIII observations are identical; $\log C = -12.0$ while the N V observations give a lower limit to $\log C$ of about -11.9 . This result is in excellent

agreement with the value found by Dupree and Goldberg who used a different technique and UV flux measurements, namely $\log C \approx -11.9$. Because of the uncertainty in the estimated value of T_c , our value of C is accurate to about a factor of 2. We conclude that $\log C = -12.0 \pm 0.3$. This gives a conductive flux from the corona into the chromosphere of $6 \cdot 10^5$ ergs/cm²/second, a value which compares favorably with the values of $5 \cdot 10^5$ and $6 \cdot 10^5$ ergs/cm/second found by Athay (1966) and Dupree and Goldberg (1967) respectively. The conductive flux found by Athay depends critically on the assumption that the coronal abundance of silicon equals the photospheric abundance and that the scaled electron pressure in the transition region P_e has a value of $6 \cdot 10^{14}$. The conductive flux found by Dupree and Goldberg depends upon a comparison of observed radio brightness temperatures and UV fluxes with the predictions of different models. They used the electron pressure given by Athay. Our new determination of the conductive flux is independent of the absolute scale of the coronal abundances and electron pressures. It is encouraging that the different techniques give similar results.

In order to obtain intensities in the K corona at 2 arc minutes above the limb that would be in agreement with the mean observed value in November 1967, an electron pressure in

the transition region P_e of about $7 \cdot 10^{14}$ is needed. Use of this electron pressure and the coronal model with $\log C = -12.0$ and $T_c = 2 \cdot 10^6$ °K gives the absolute abundances presented in Table 2. Photospheric values, Athay's values and Pottasch's values are presented for comparison. Considering the uncertainties in the instrumental calibration and the model for which the abundances were determined, our abundances are probably accurate at best to within a factor of 2 to 3. Thus it is premature to conclude on the basis of our results alone that the coronal and photospheric abundances differ for the elements considered here. In a future paper we shall describe results of a more detailed analyses of UV and K-coronameter observations.

Note that all of the results given in this paper depend critically on the assumption that the corona is stratified. If the temperatures and densities of coronal inhomogeneities in the equatorial region depart significantly from the values in the mean model and if these inhomogeneities cover a substantial fraction of the solar disk, these differences will have an important effect on the relative intensities of different coronal lines. However, since the adopted model gives reasonable coronal temperatures, temperature gradients, and abundances, the model should also give a good approximation of the mean conditions in the equatorial chromospheric-coronal transition

region and lower corona. In future papers we shall compare this model with OSO-IV observations of a number of other UV lines.

Acknowledgements

I would like to thank Dr. L. Goldberg, Dr. R.W. Noyes, Dr. W.H. Parkinson, Dr. E.M. Reeves, and other personnel of the Harvard Solar Satellite Project whose efforts produced such a fine OSO experiment and set of observations. I would also like to express my appreciation to them and Dr. A.K. Dupree for many stimulating discussions. This work was supported by the National Aeronautics and Space Administration through contract NASw-184.

References

- ALLEN, J.W. and DUPREE, A.K.: 1969, Astrophys. J. 155, 27.
- ATHAY, R.G.: 1966, Astrophys. J. 145, 784.
- AVRETT, E.H. and HUMMER, D.G.: 1965, Mon. Not. Roy. Astr. Soc. 130, 295.
- BILLINGS, D.E.: 1966, A Guide to the Solar Corona (New York: Academic Press).
- CHAPMAN, S.: 1954, Astrophys. J. 120, 151.
- DUPREE, A.K. and GOLDBERG, L.: 1967, Solar Phys. 1, 229.
- GOLDBERG, L., MULLER, E. and ALLER, L.H.: 1960, Astrophys. J. Suppl. 5, 1.
- GOLDBERG, L., NOYES, R.W., PARKINSON, W.H., REEVES, E.M. and WITHBROE, G.L.: 1968, Science, 162, 95.
- JORDAN, D.: 1966, Mon. Not. Roy. Astr. Soc. 132, 463.
- NEWKIRK, G.: 1967, Ann. Rev. Astron. and Astrophys. 5, 213.
- POTTASCH, S.R.: 1967, Bull. Astron. Inst. Netherlands 19, 113.
- SEATON, M.J.: 1964, Plan. Space Sci. 12, 55.
- VAN DE HULST, H.C.: 1950, Bull. Astron. Inst. Netherlands 11, 135.
- WIESE, W.L., SMITH, and GLENNON, B.M.: 1966, Atomic Transition Probabilities, Vol. 1 Hydrogen Through Neon, U.S. Dept. of Commerce, Nat. Bur. Standards.
- WOOD, A. and DUPREE, A.K.: 1969, private communication.
- ZIRIN, A.: 1966 The Solar Atmosphere (Waltham, Mass.: Blaisdell Publishing Co.).

TABLE 1

Spectral Line Information

ION	λ (Å)	g(**)	f	I_0 (erg/cm ² /sec/sterad)	T_{\max} (°K)
N V	1238.8	0.78	0.156 [†]	$1.5 \cdot 10^{-3}$	$2.0 \cdot 10^5$
O VI	1031.9	0.8	0.131 [†]	$9.7 \cdot 10^{-3}$	$3.3 \cdot 10^5$
Ne VIII	770.4	0.89	0.102 [†]	$1.0 \cdot 10^{-3}$	$7.1 \cdot 10^5$
Mg X	625.3	0.96	0.045*	$1.1 \cdot 10^{-3}$	$1.3 \cdot 10^6$
Si XII	499.3	0.88	0.069**	$1.3 \cdot 10^{-3}$	$2.2 \cdot 10^6$

* 1. Dupree and Goldberg 1967

** 2. Pottasch 1967

† 3. Wiese, Smith, and Glennon, 1966.

TABLE 2

Abundances ($\log N_a/N_H$)

Element	Previous Abundance Determinations		Abundances from this investigation	
	Photosphere Goldberg et al. (1960)	Athay (1966) Coronal Abundance Pottasch (1967)	Modified Dupree & Goldberg model	Adopted model *
N	-4.02	-3.97	-3.48	-3.52
O	-3.05	-3.39	-2.91	-2.97
Ne	-----	-4.5	-4.08	-4.17
Mg	-4.60	-4.5	-3.88	-3.99
Si	-4.50	-4.5	-3.73	-3.98

* $\log C = 12.0$, $\log T_C = 6.3$, $P_0 = 7.10^{14}$

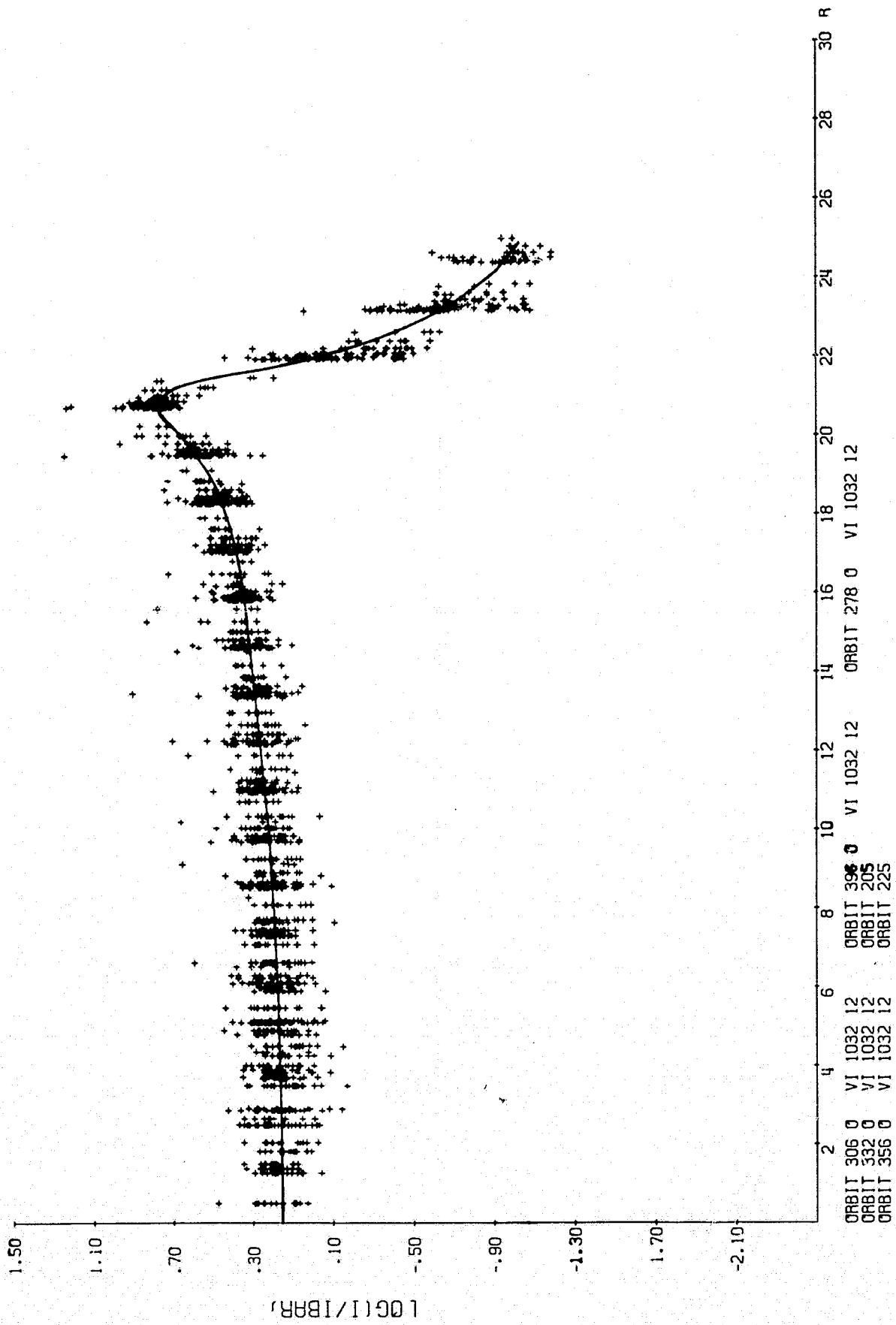


FIG. 1

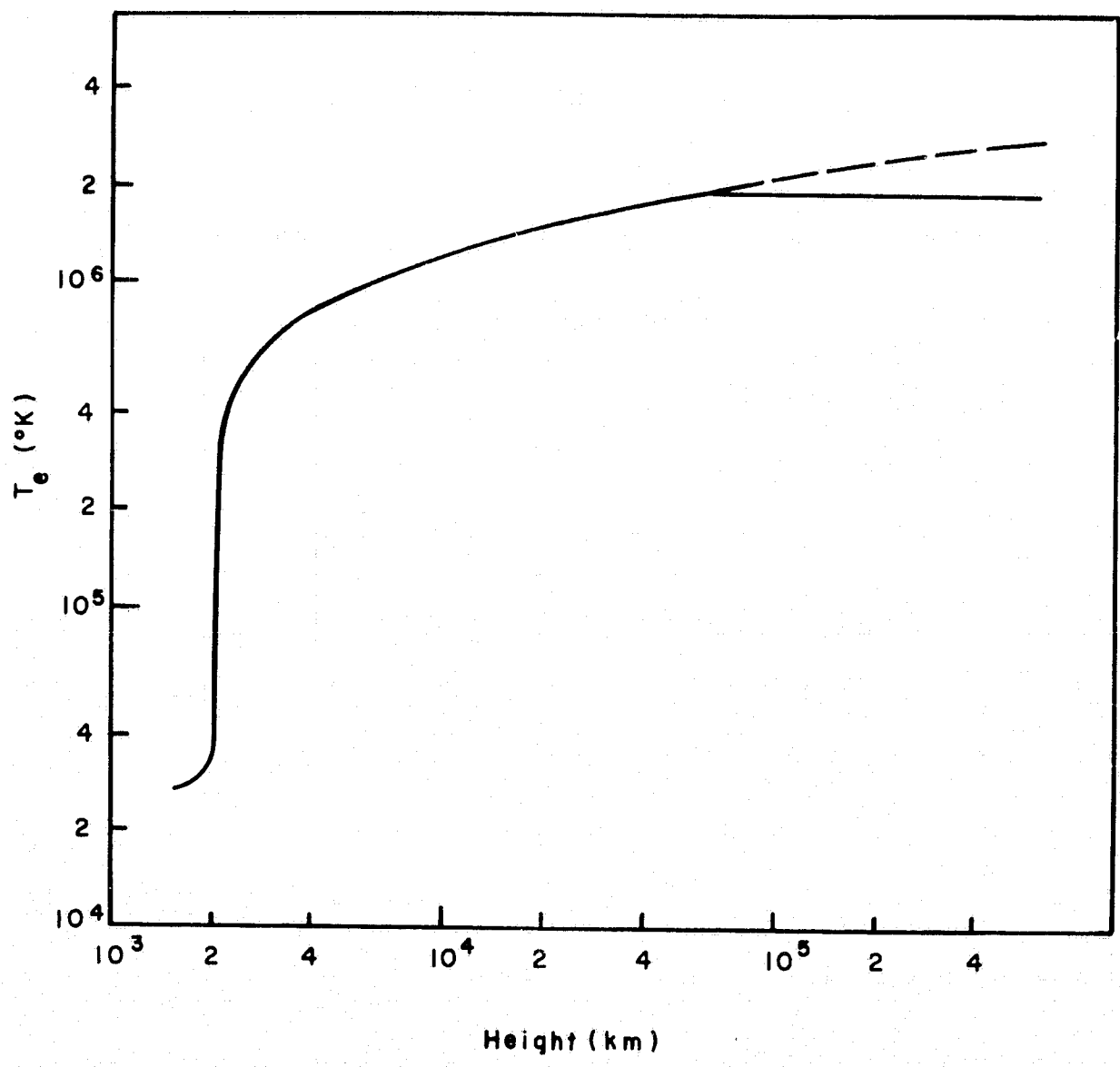


FIG. 2

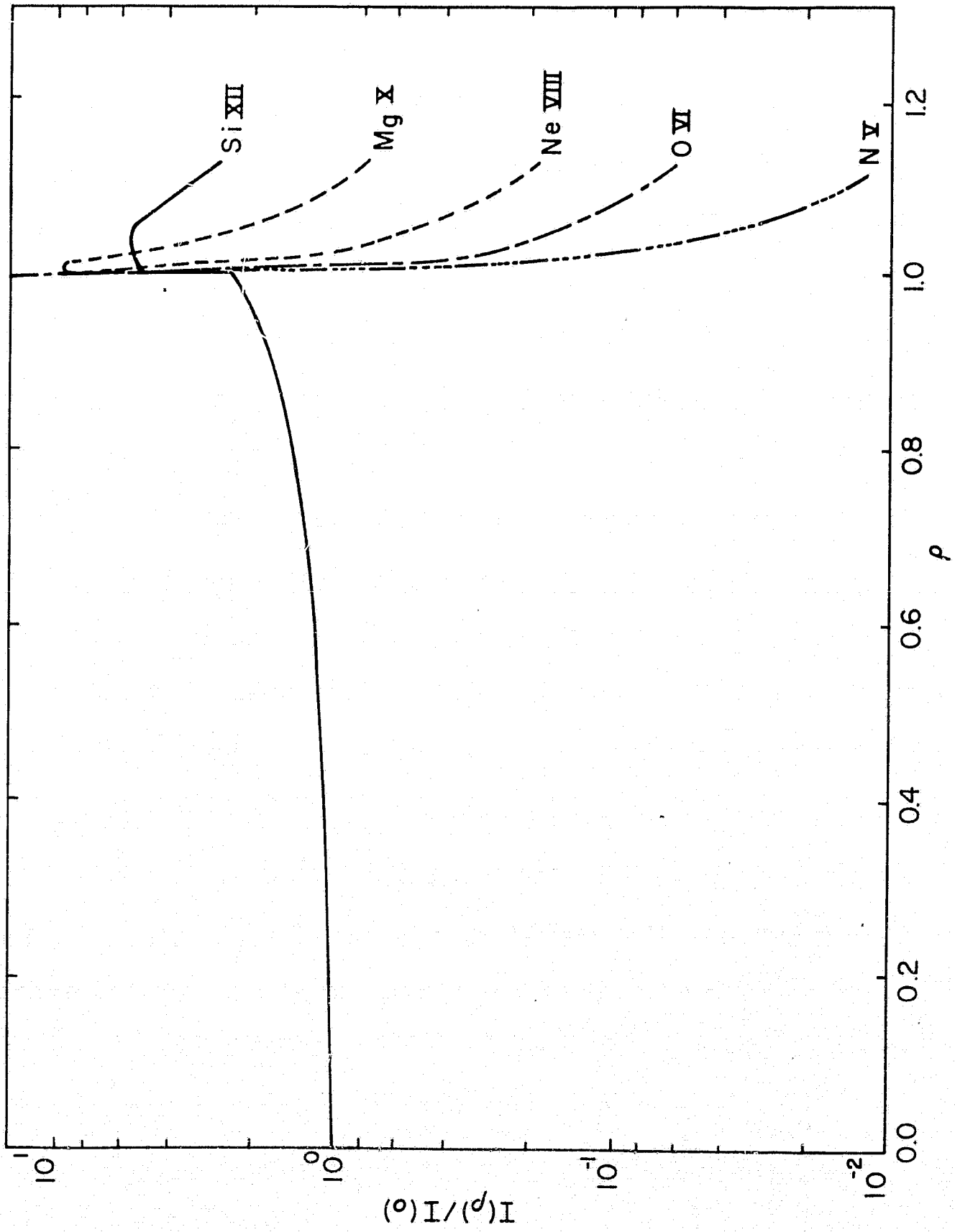


FIG. 3

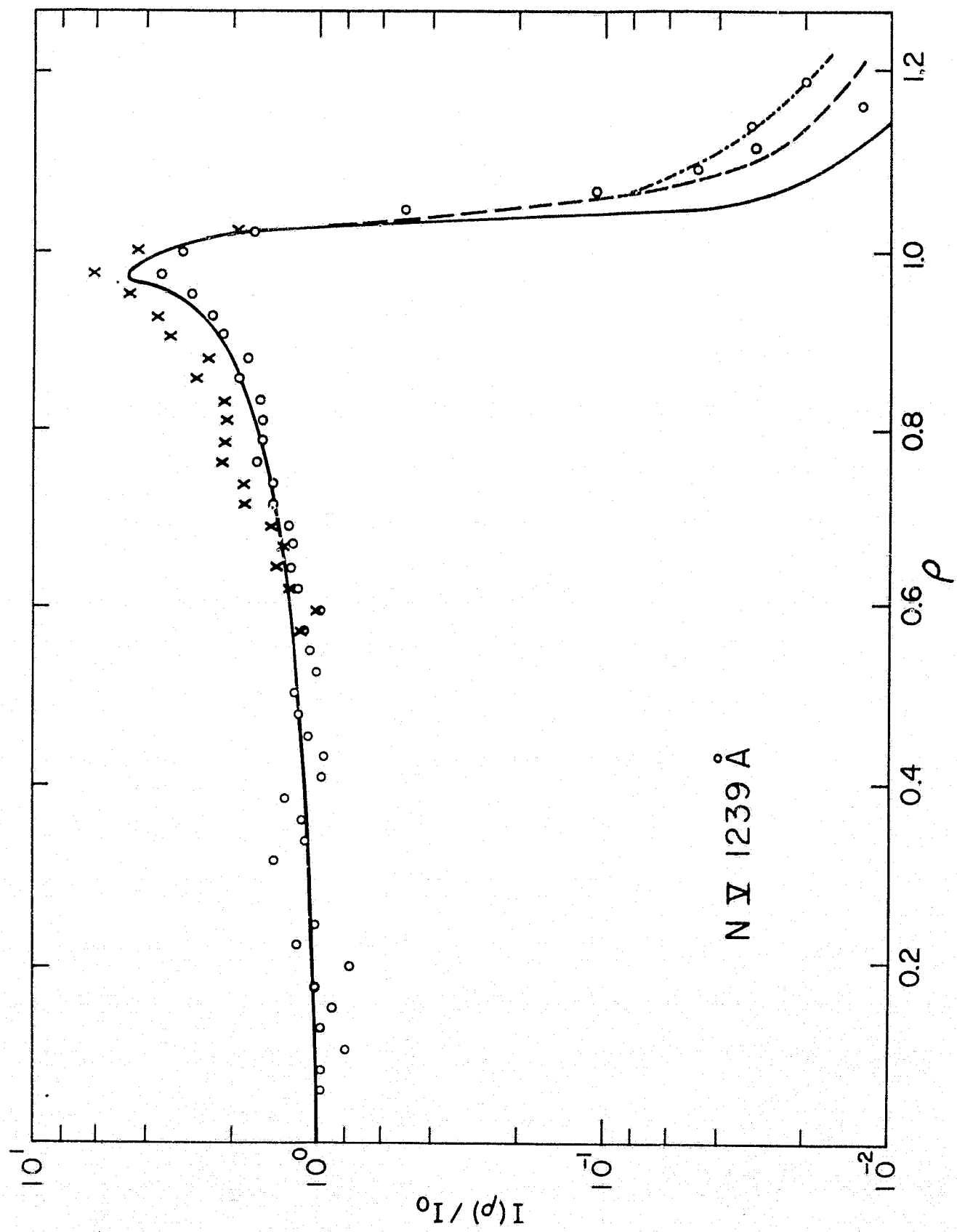


FIG. 4

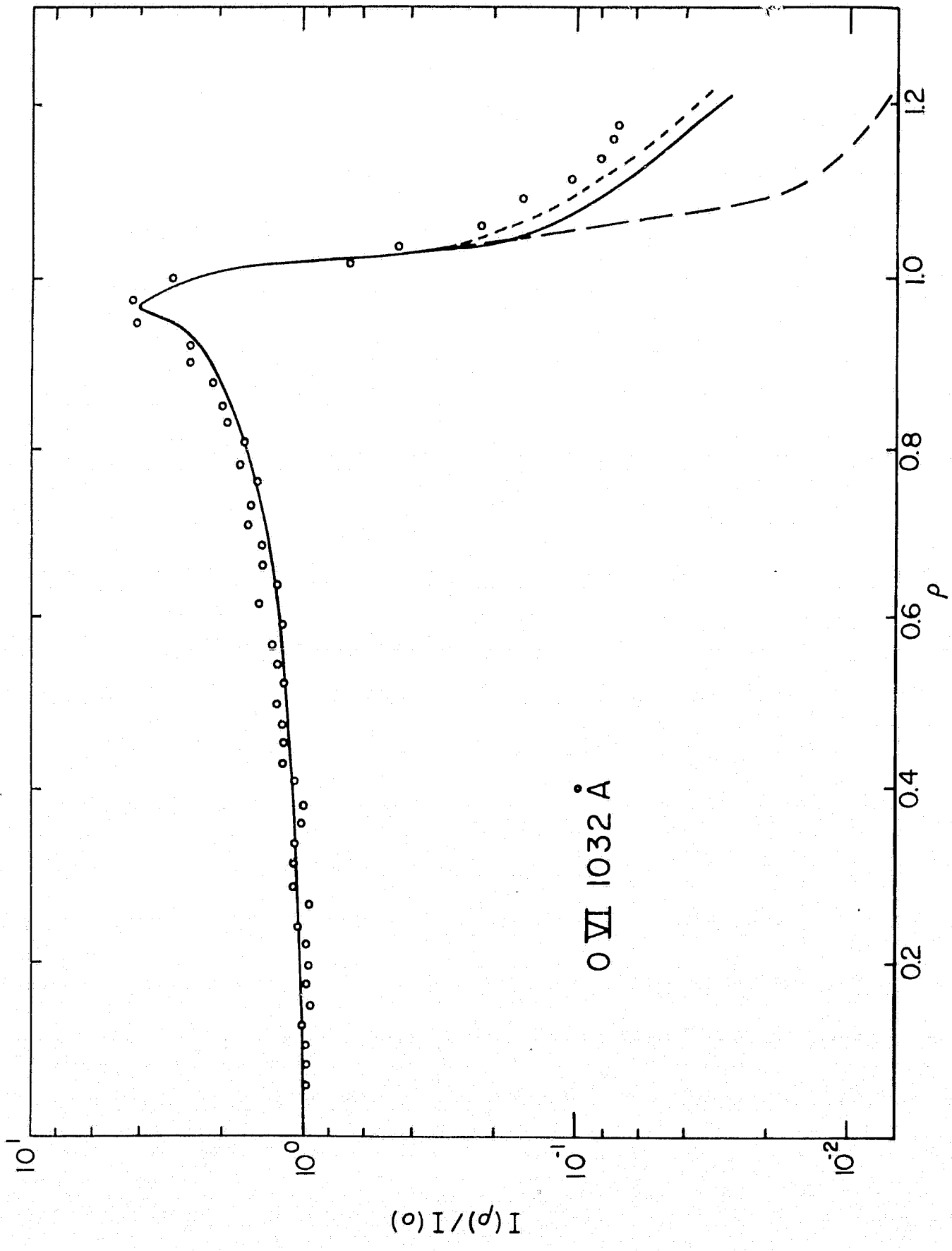


FIG. 5

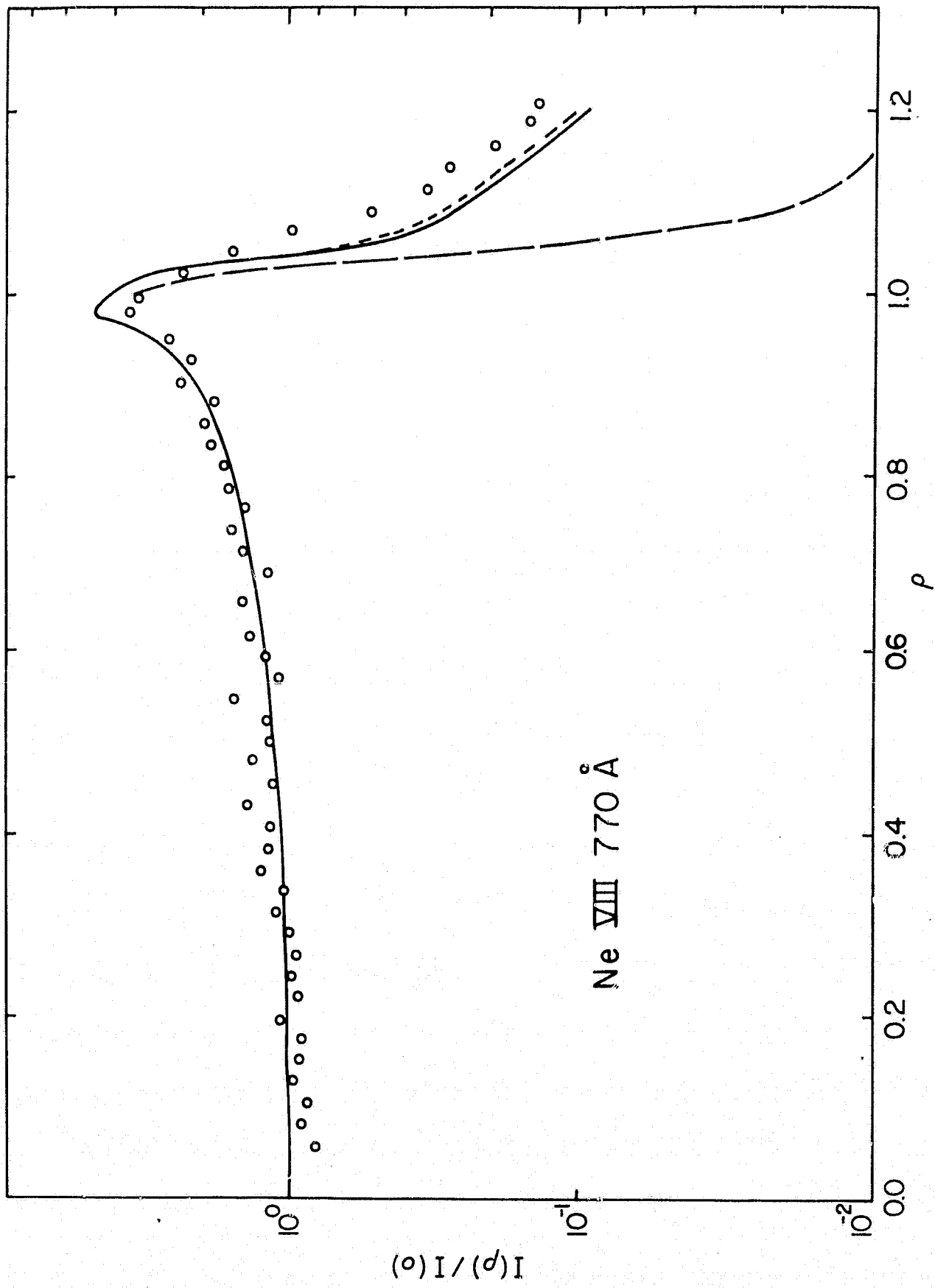
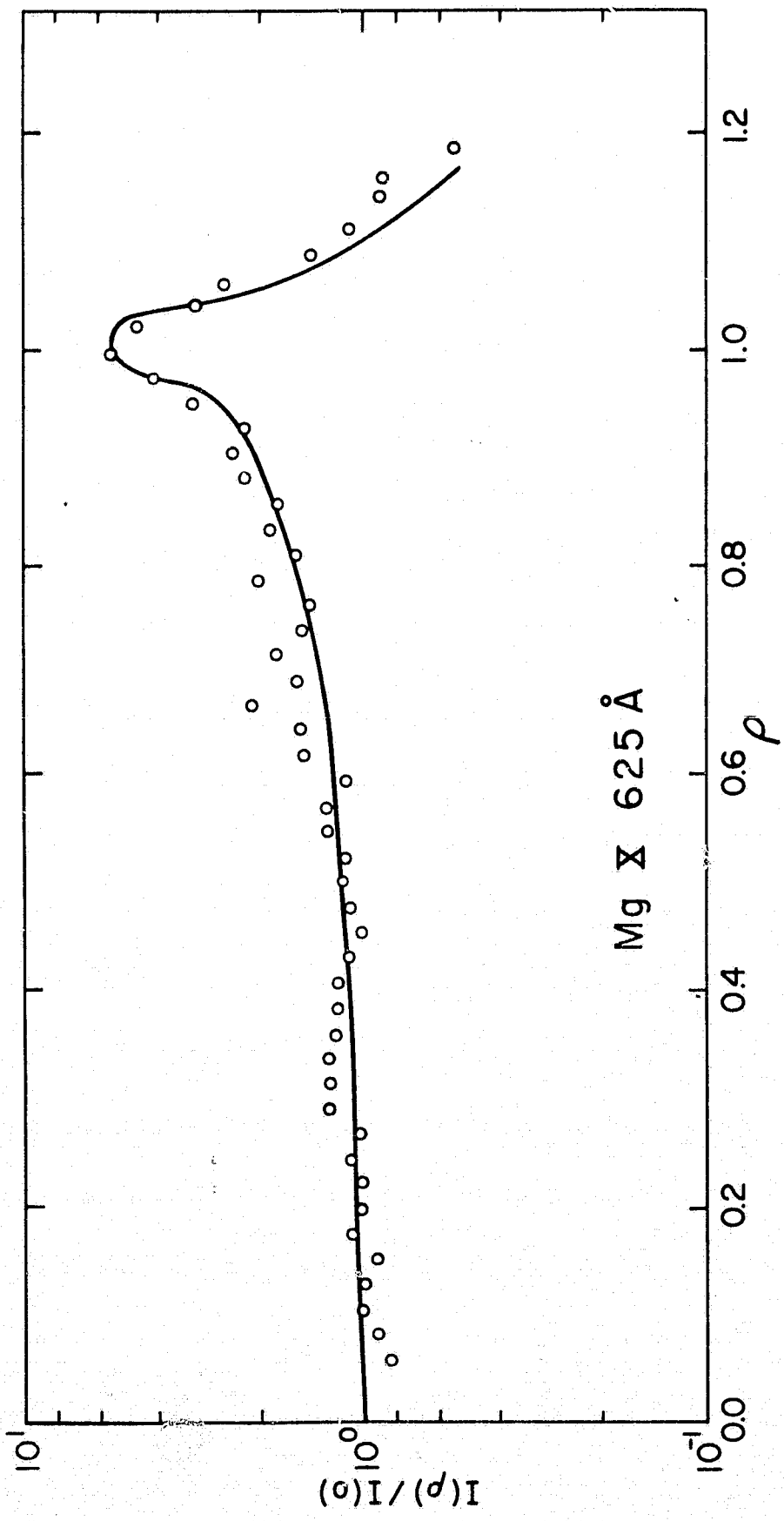


FIG. 6



Mg X 625 Å

FIG. 7

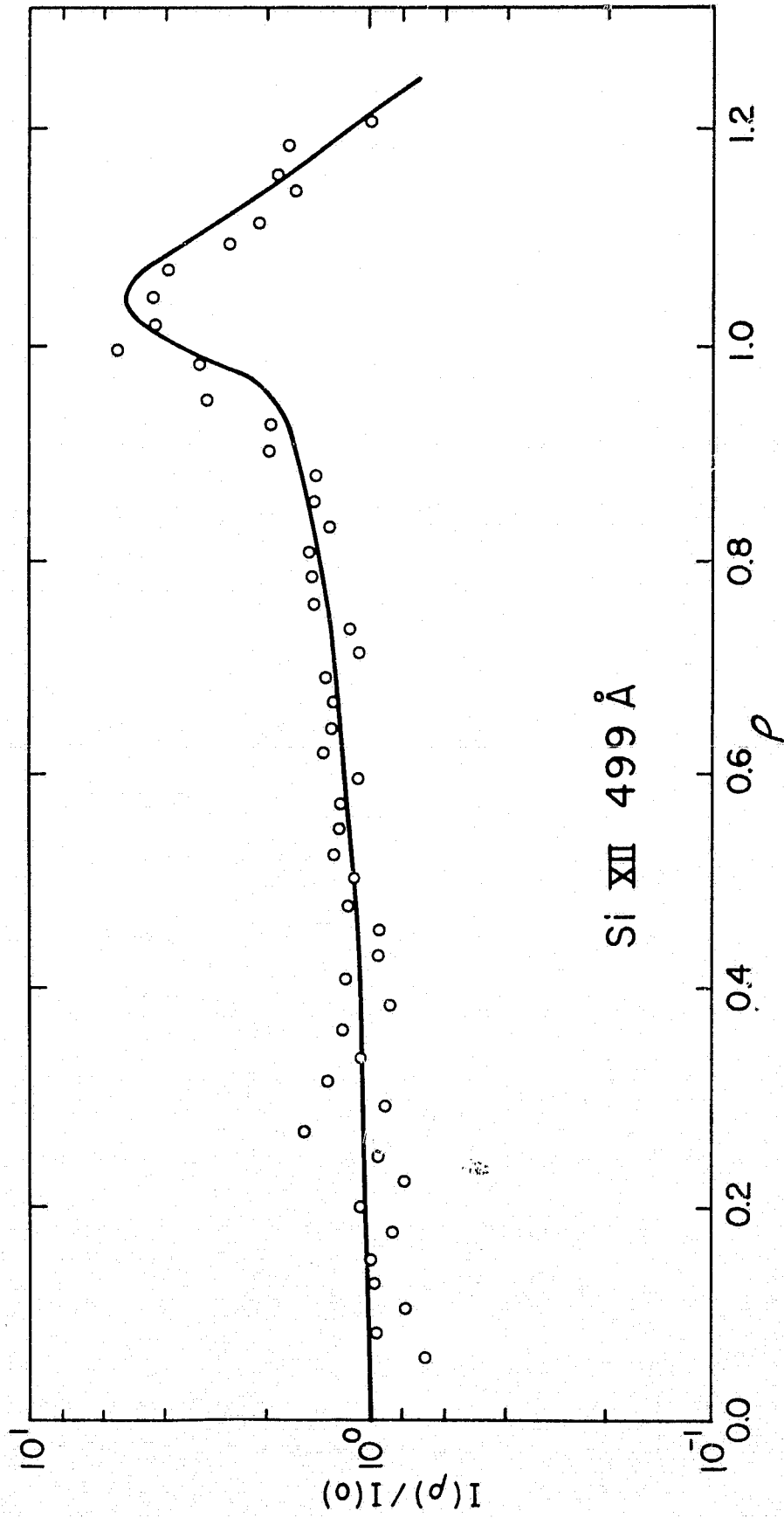


FIG. 8

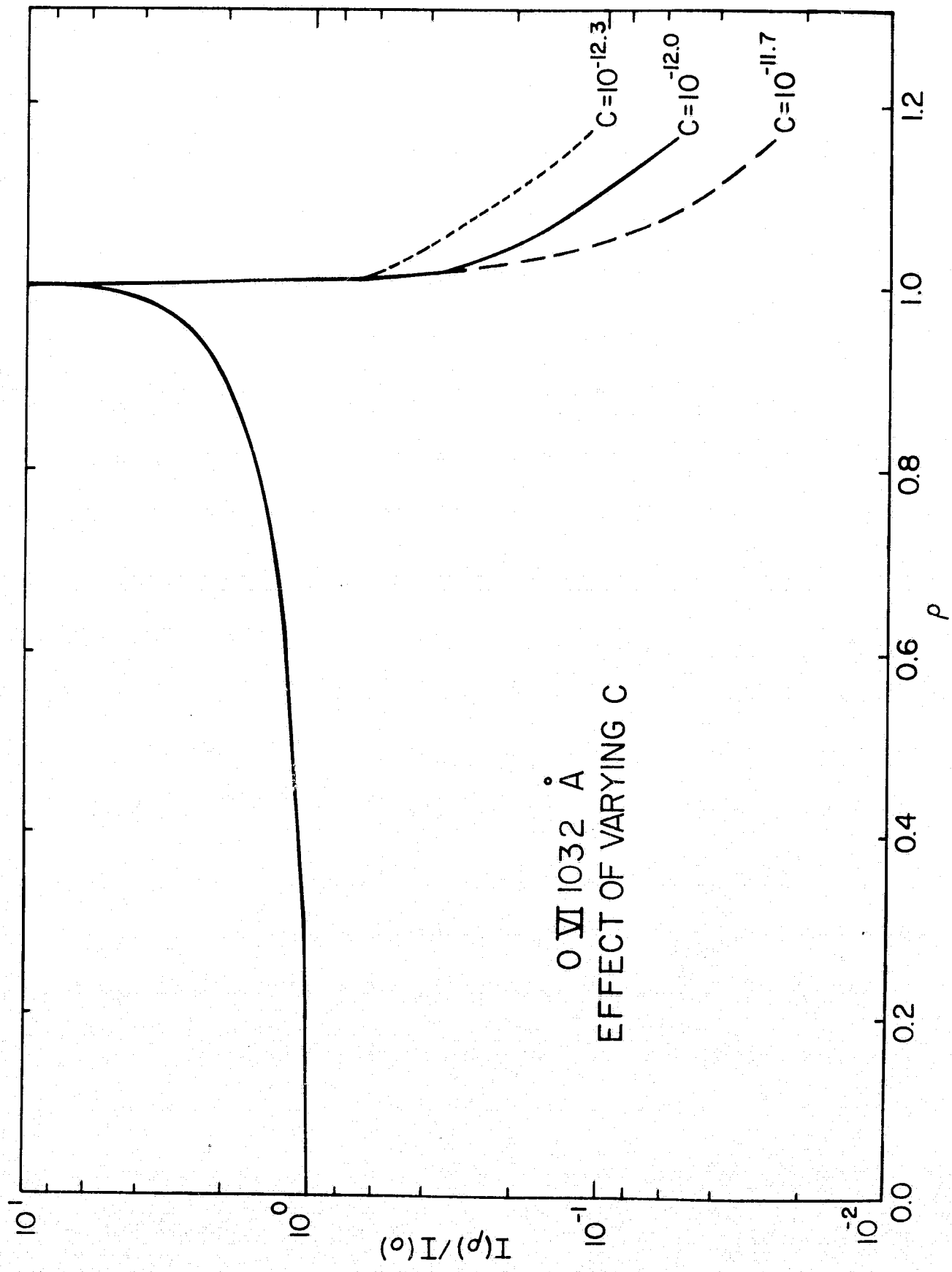


FIG. 9

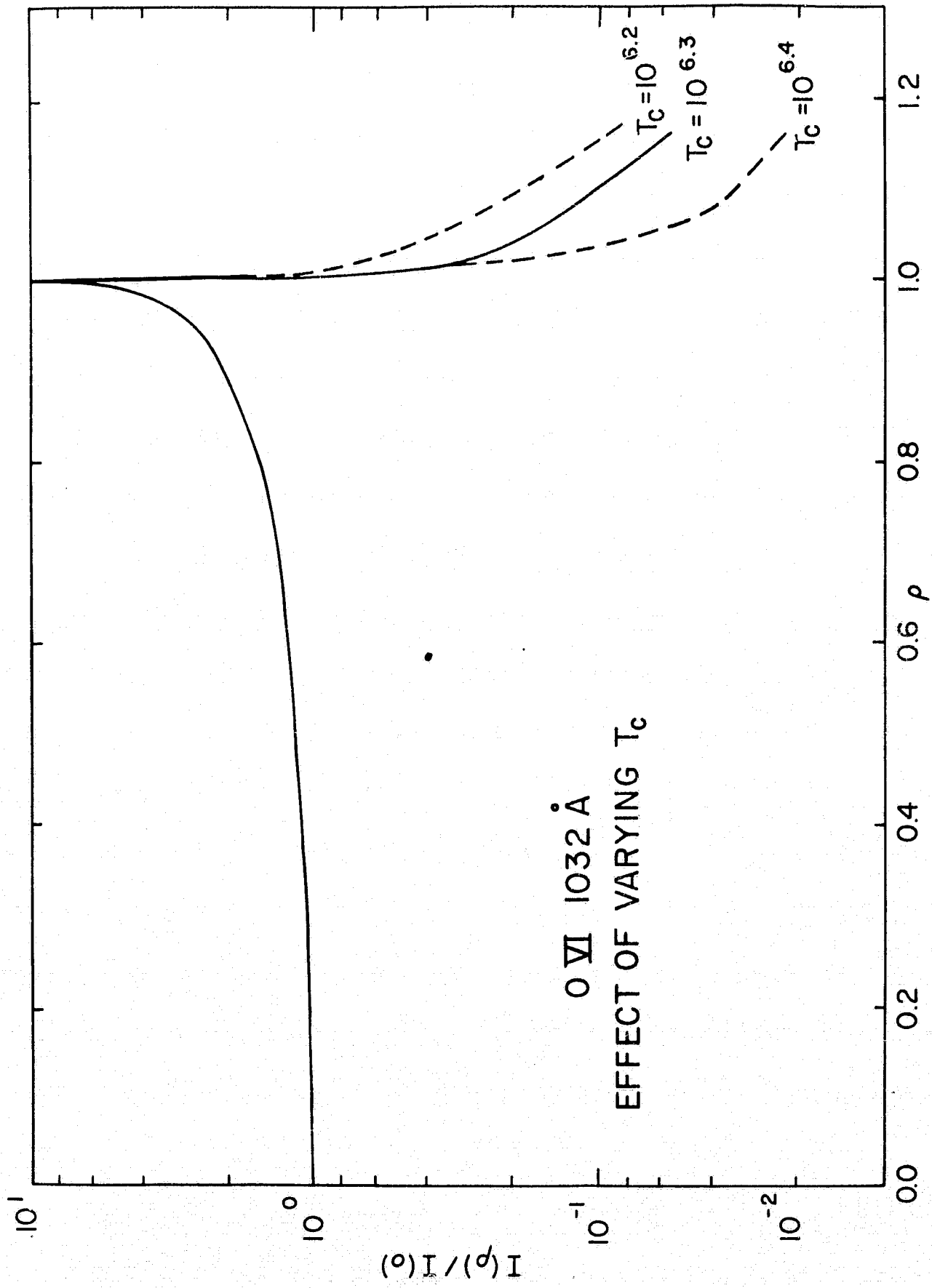


FIG. 10

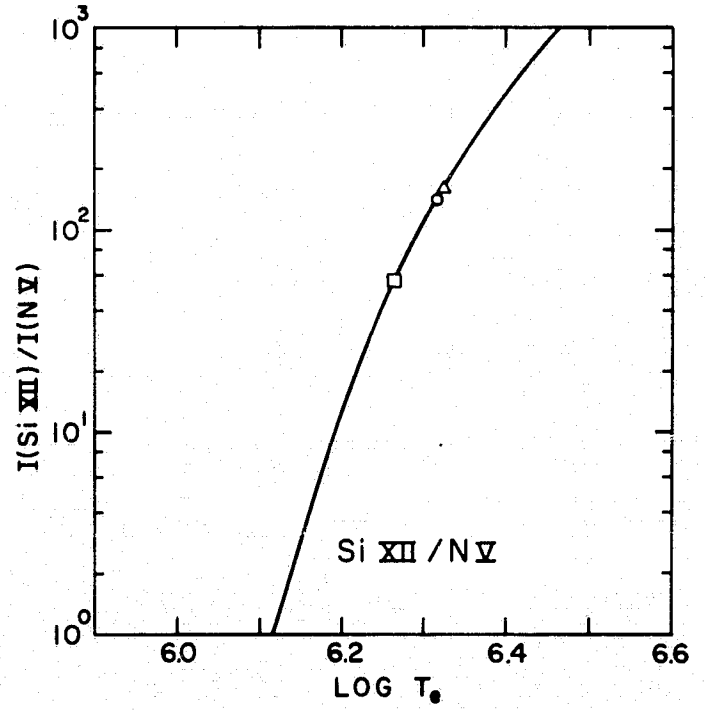
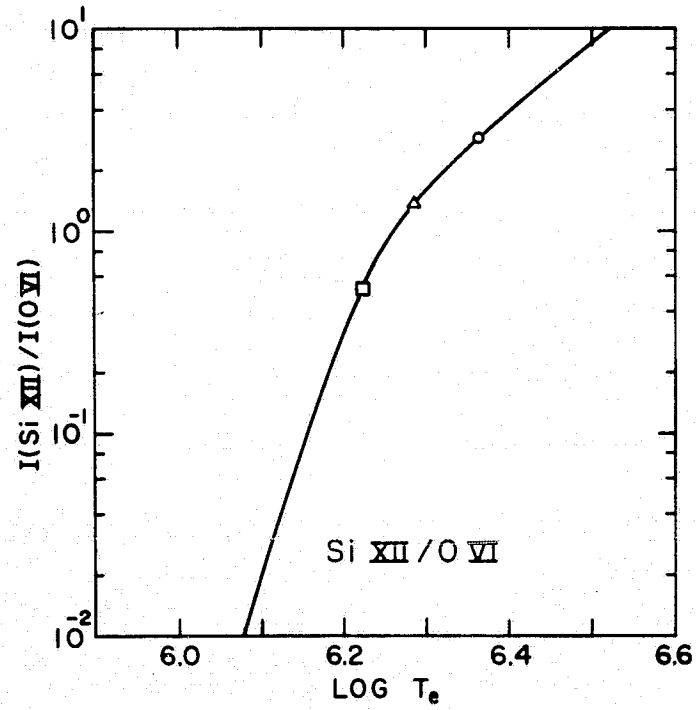
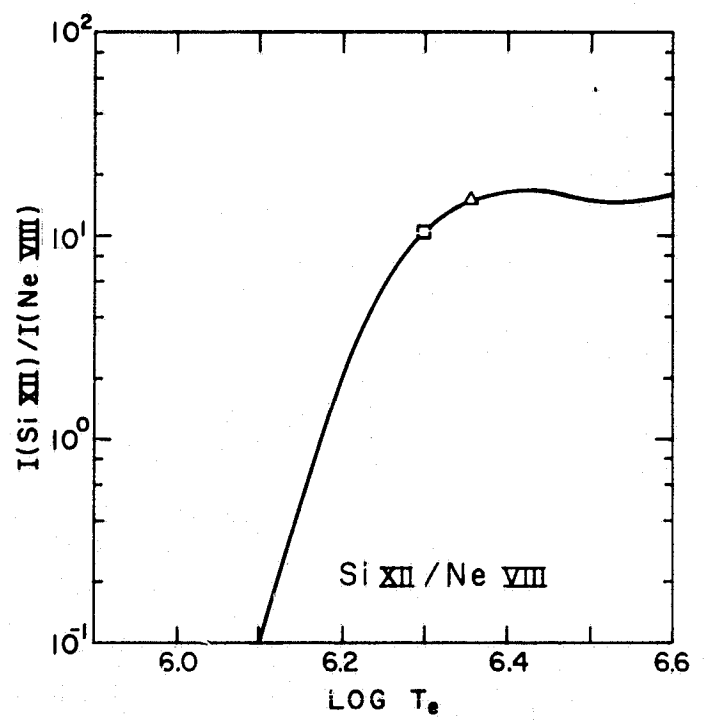
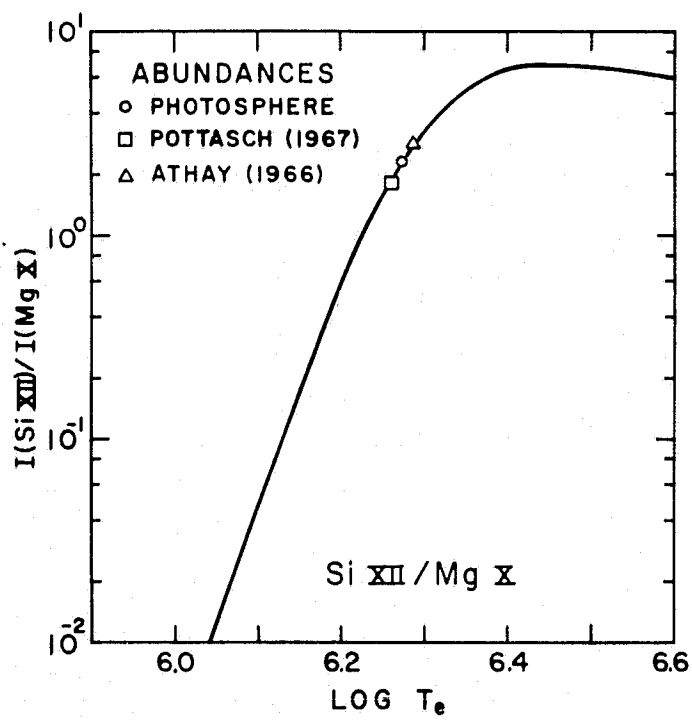


FIG. II

Figure Captions

- Figure 1. The center to limb variation of the O VI intensity at $\lambda 1032$. The ordinate is proportional to the logarithm of the intensity in a one arc minute square area. The abscissa gives the distance from the center of the disk in arbitrary units. The solid line is the mean curve obtained from the data. The mean curve is determined by averaging points at intervals of 0.5 units along the abscissa.
- Figure 2. The dependence of the electron temperature on height for the modified Dupree and Goldberg model (see text) is given by the solid line. The dashed line represents the temperatures in the higher layers of the corona as given by Dupree and Goldberg.
- Figure 3. The center to limb variation of the intensity for resonance lines of the lithium-like ions N V, O VI, Ne VIII, Mg X, and Si XII. These curves were computed with the modified Dupree and Goldberg model.
- Figure 4. The center to limb variation of the intensity for $\lambda 1239$ of N VI. A continuum at 1239\AA has been subtracted from the $\lambda 1239$ data, with two assumptions.
- (1) That the continuum varies as $1/\mu$ (points) and
 - (2) that the continuum does not vary from center to

limb (crosses). The solid line is the limb brightening calculated with the Dupree and Goldberg model and includes the smoothing caused by the one arc minute entrance slit of the instrument. The dashed line is the measured limb profile for a spectral line with no coronal emission. The dotted line is the sum of the first two curves and is the predicted limb brightening for $\lambda 1239$ of N V.

- Figure 5. The center to limb variation of the intensity for $\lambda 1032$ of O VI. The points are the observed values. The theoretical curves are the same as in Figure 4.
- Figure 6. Same as figure 5 but for $\lambda 770$ of Ne VIII.
- Figure 7. The center to limb variation of the intensity for $\lambda 625$ of Mg X. The solid curve is the variation predicted by the modified Dupree and Goldberg model.
- Figure 8. Same as figure 7 but for $\lambda 499$ of Si XII.
- Figure 9. The effect on the limb brightening for the O VI line where the constant C is varied (see text).
- Figure 10. The effect on the limb brightening for O VI line when the temperature of the corona T_c is varied.
- Figure 11. A comparison between the predicted and observed ratios of resonance lines of the lithium-like ions. The circles compare the observed ratios with the ratios

predicted for photospheric abundances. The squares represent the ratios when Pottasch's (1967) abundances are used. The triangles represent the ratios when Athay's (1966) abundances are used.

PART II

LINES FORMED IN THE CHROMOSPHERIC-CORONAL

TRANSITION REGION

PRECEDING PAGE BLANK NOT FILMED.

1. Introduction

In an earlier paper, hereinafter called Paper I, Withbroe (1969) described an analysis of limb brightening observations of resonance lines of the lithium-like ions N V, O VI, Ne VIII, Mg X, and Si XII, and showed that the limb brightening for these lines could be explained with a coronal model very similar to that derived by Dupree and Goldberg (1967). The present paper extends the analysis to include lines of ions such as C III, N III, N IV, O III, O IV, O V, and Si IV. In order to explain the observations it appears necessary to include in the model the effects of spicules that extend up into the chromospheric-coronal transition region.

2. Observations

The method used to obtain limb-brightening curves is described in Paper I, and may be summarized briefly. The observations were obtained in October and November 1967 with the Harvard spectrometer-spectroheliometer on OSO-IV. The measurements consist of spectroheliograms made up of a 48 x 40 array of points. The spatial resolution of the data is one arc minute. Curves were generated for the equatorial region

between solar latitudes $\pm 10^\circ$ and -10° . Use of data in this range of latitudes gave sufficient points to produce smooth limb-brightening curves and yet avoided most active regions.

3. Theory

Most of the equations needed to analyze the observations appear in Paper I, and are useful primarily when the total optical thickness of the line-forming region is small, less than unity. One of the lines considered here, the C III line at 977\AA , has an optical depth of about unity. To insure that the approximations used in Paper I can be used for this line, source functions were determined by solving the equation of transfer with an iterative procedure. Intensities computed with the resulting source functions agreed to within a few per cent of the intensities computed with the equations given in Paper I.

To indicate how the optical thickness, τ , of the line-forming region affects the limb brightening of UV lines, first we define a scaled optical depth $\tau = \sqrt{\pi} \cdot \tau_0$, where τ_0 is the total optical thickness of the line-forming region at the center of the line. The observed parameter is the intensity in the line

integrated over frequency, $I(\rho)$, where ρ is the distance from the center of the solar disk to the intersection of the line of sight with the solar disk in units of R_{\odot} , the radius of the sun. From Paper I we have

$$I(\rho) = \int_{-\infty}^{\infty} I_{\nu}(\rho) d\nu \quad , \quad (1)$$

$$= \Delta\nu_0 \int_0^{\tau} S(t) \cdot \Phi(t/\mu) \cdot dt/\mu \quad , \quad (2)$$

where

$$\Phi(t/\mu) = \int_{-\infty}^{\infty} \phi_x \cdot e^{-\phi_x t} \cdot dx \quad , \quad (3)$$

$x = \Delta\nu/\Delta\nu_0$, $\Delta\nu$ is the distance from the center of the line in frequency units, $\Delta\nu_0$ is the Doppler width which is assumed to be constant over the region of line formation, and ϕ_x is the normalized Doppler broadening function. The geometrical term

$$\mu = \sqrt{1-\rho^2}$$

for lines formed very close to the surface of the sun. As is shown in Paper I, the source function, $S(t)$, and the optical depth, t , can be determined for any coronal model giving

electron densities and the temperatures as a function of height.

If the optical thickness of the line-forming region, τ , is very small, the intensity of an emission line will vary as $1/\mu$. As τ increases the intensity at the limb $I(\rho \approx 1)$ will be decreased with respect to the intensity at the center of the disk, $I(\rho = 0)$. For lines with optical depths larger than about 0.1 the limb brightening depends critically on τ . Figure 1 shows an example for a line where $S(t)$ equals a constant for $t \leq \tau$ and equals 0 for $t > \tau$. The limb brightening curves have been smoothed with the OSO-IV aperture function in order to obtain curves that can be directly compared to the OSO-IV observations. When the optical thickness of the line-forming region is the order of unity or larger, the depth dependence of the source function may also influence the shape of the limb brightening curves.

It is possible to estimate the optical depth in XUV lines even if the abundances and f -values for the lines are not accurately known. From equation (13) of Paper I we obtain

$$\tau = 2.12 \cdot 10^{-2} \frac{A \cdot f \cdot P_e}{\Delta v_0} \int_{T_1}^{T_2} R_i(T_e) \left(\frac{dT_e}{dh} \right)^{-1} T_e^{-1} dT_e, \quad (4)$$

for lines formed in the chromospheric-coronal transition region. The temperatures T_1 and T_2 are those of the chromosphere and the corona respectively. The quantity $R_i(T_e)$ is the ratio n_i/n_a , where n_i is the number of ions (cm^{-3}) of the type producing the line and n_a is the total number of atoms (cm^{-3}) of the element summed over all stages of ionization, $A = n_a/n_H$ is the abundance of the element with respect to hydrogen, f is the oscillator strength, and (dT/dh) is the temperature gradient. In writing equation (4) it is assumed that the quantity $P_e = n_e T_e$ is constant over the line-forming region. This is an excellent approximation for lines formed in the transition region, since the geometrical thickness of this layer is small compared to the pressure scale height. From equation (18) of Paper I we also obtain for the flux emitted in a UV line

$$F = 2.38 \cdot 10^{-20} A \cdot f \cdot g \cdot P_e^2 \int_{T_1}^{T_2} R_i 10^{(-5040 W/T_e)} T_e^{-5/2} \left(\frac{dT}{dh}\right)^{-1} dT_e \quad (5)$$

The quantity W is the excitation potential of the line in volts and g is the mean Gaunt factor.

From equations (4) and (5) we obtain

$$\tau = 8.9 \cdot 10^{17} \cdot \frac{F}{g P_e} \frac{1}{\Delta \nu_0} \frac{\int_{T_1}^{T_2} R_i T_e^{-1} \left(\frac{dT}{dh}\right)^{-1} dT_e}{\int_{T_1}^{T_2} R_i T_e^{-5/2} 10^{-5040 W/T_e} \left(\frac{dT}{dh}\right)^{-1} dT_e} \quad (6)$$

Since the ratio of the two integrals is relatively insensitive to the adopted coronal model, τ depends primarily on the emergent flux in the line and the electron pressure in the transition region.

The coronal model used is a modification of a model derived by Dupree and Goldberg (1967) from an analysis of the solar flux emitted in the XUV spectral lines of O, Si, and Fe ions. For the chromospheric-coronal transition region, $T_e < 2 \cdot 10^6$ K, we used the same variation of temperature with height as that given by Dupree and Goldberg. To this transition region was attached a corona with a temperature equal to 2 million degrees K. The scaled pressure, $P_e = n_e T_e$, at the height where $T_e = 10^5$ K was set at $6 \cdot 10^{14}$. The electron pressures and densities at other heights were determined from the equation of hydrostatic equilibrium. Paper I demonstrates that this model explains the limb brightening in the resonance lines of the lithium-like ions N V, O VI, Ne VIII, Mg X, and Si XII. These ions are formed at temperatures ranging from $2 \cdot 10^5$ to $2.5 \cdot 10^6$ K.

4. Results

Table 1 gives optical depths for a number of lines determined from equation (6), from the modified Dupree-Goldberg model, and from fluxes determined from OSO-IV data. For most lines the

predicted optical thickness of the line-forming region is small, of the order of 0.1. As is shown in Section 3, this implies that these lines should have limb-brightening curves which vary nearly as $1/\mu$. The fourth column in Table 1 gives the number of spectroheliograms used to construct the limb-brightening curves to be shown later. Each spectroheliogram was obtained by averaging data from one orbit (cf. Paper I).

Limb-brightening curves have been calculated for the lines listed in Table 1. The calculations were made with equation (2), the modified Dupree-Goldberg model, and optical depths which were scaled so as to give the correct total optical thickness of the line-forming region (eq. 6). The calculated limb brightening agrees fairly well with the observations for $\lambda 977$ of C III, $\lambda 991$ of N III, $\lambda 1394$ of Si IV, $\lambda 1239$ of N V, $\lambda 1032$ of O VI, $\lambda 770$ of Ne VIII, $\lambda 625$ of Mg X, and $\lambda 499$ of Si XII. The N V, O VI, Ne VIII, Mg X, and Si XII limb-brightening data are discussed in Paper I. Limb brightening curves for the other three lines are given in Figures 2, 3, and 4. The circles are the observed values and the solid lines are the limb brightening predictions of the model. The theoretical limb brightening curves have been smoothed with the OSO-IV aperture function.

The $\lambda 1394$ line of Si IV is located on top of a continuum whose limb brightening was not observed. Because this continuum contributes about 25% of the intensity at 1394\AA , the exact shape of the limb brightening curve is not known for the Si IV line. The theoretical curve in Figure 2 assumes that the continuum has the same limb brightening as the Si IV line and, therefore, varies nearly as $1/\mu$. As was mentioned in Paper I, the limb brightening of the N V line at $\lambda 1239$ is also somewhat uncertain for this reason. However, at 991\AA the continuum contributes only 10% of the total intensity and therefore should not affect the limb brightening of the N III line very much. The $\lambda 991$ line, like $\lambda 1032$ of O VI (cf. Paper I) has a limb brightening which varies very nearly as $1/\mu$ as is predicted (see Fig 3). The $\lambda 977$ line of C III is predicted to have an optical depth sufficiently large that its brightening toward the limb should be less than for the other lines. This is shown in Figure 4. The solid line shows the limb brightening predicted by the model, the dotted line shows that for an optically thin line.

For the remaining lines in Table 1, $\lambda 703$ of O III, $\lambda 630$ of O V, $\lambda 554$ of O IV, and $\lambda 765$ of N IV, the predicted and observed limb-brightening curves do not agree. In all cases

the observed ratio $I(\rho)/I(\rho = 0)$ at the limb is significantly smaller than the predicted values, as shown in Figures 5-8. For the N IV line at 765\AA , which lies on top of the Lyman continuum, the intensity of the continuum has been removed through use of center-to-limb observations made in the continuum at a nearby wavelength.

The lack of agreement between the predicted and observed limb brightening for the O III, O IV, O V, and N IV lines may result from several factors. The approximations used in calculating the theoretical optical depths and limb-brightening curves could be inadequate. However, the same theory successfully explains the observations of a number of other lines, one of which, the C III line at 977\AA , has the largest optical depth of all lines studied. To account for the agreement or disagreement of the predicted and observed behavior for each line by using a more sophisticated theory would require a substantial effort.

Another possibility is to use a model containing inhomogeneities. The lines considered here are formed in the chromospheric-coronal transition region. This region appears to be strongly influenced by the structure of the chromospheric network, as is shown by the observations of Purcell and Tousey (1969) who obtained photographic spectroheliograms in the

lines $\lambda 304$ of He II, $\lambda 554$ of O IV, and $\lambda 630$ of O V. The spectroheliograms were obtained with an instrument launched on a rocket and have excellent spatial resolution, of the order of 10 arc seconds. They show that much of the emission in the He II, O IV, and O V lines is concentrated in a network structure similar to the chromospheric network. This suggests that the transition region might be better represented by a two-component model that has one density and temperature structure in the network and a different structure in the inter-network areas. With an inhomogeneous model, which has more free parameters than the simple homogeneous stratified model used in the present calculations, it is possible to obtain optical depths significantly different from those given in Table 1. If the optical depths of the O III, O IV, O V, and N IV lines can be increased substantially, by an order of magnitude or so, then it is possible to explain their limb brightening. The derivation of a successful inhomogeneous model will be difficult. It must, for example, explain the differences in the O V and O VI lines, which are formed at nearly the same temperature and are predicted to have almost identical optical depths in the homogeneous model.

A simpler solution to the problem also makes use of inhomogeneities, but in a different manner. It is significant that all of the lines whose limb brightening is unexplained by the Dupree-Goldberg model have wavelengths less than 912\AA , the wavelength at the head of the Lyman continuum. These lines, $\lambda 703$ of O III, $\lambda 554$ of O IV, $\lambda 630$ of O V, and $\lambda 765$ of N IV, are also formed in the transition region. On the basis of an analysis of UV and visible lines of hydrogen, He I, and He II, Athay (1966) concluded that the transition region, a geometrically thin layer, is located at a height of 2000 km. The Dupree-Goldberg model, which was developed by use of some of Athay's techniques, retains this feature of Athay's model. A height of 2000 km is well below the average height of spicules and other features observed in H α with ground-based telescopes. Viewed from a vertical perspective, spicules cover only a few percent of the solar surface. However, because they are elongated features, the fraction of the disk they cover rapidly increases as the angle between the normal to the surface and the line of sight, θ , increases, until at the limb the observer sees a surface covered almost entirely by spicules. Thus, if spicules are opaque to radiation at wavelengths capable of being absorbed by the Lyman continuum, spicular absorption can significantly modify the limb brightening of UV lines emitted in layers

below the tops of spicules.

Giovanelli's (1967) calculations of the excitation of hydrogen under chromospheric conditions suggest that spicules may be optically thick in the hydrogen Lyman continuum. For example, calculations for a layer 2000 km thick with $n_e = 10^{11}$ and $T_e = 10^4$ K give the optical depth as about 10 at the head of the Lyman continuum (912Å). Higher temperatures give smaller optical depths while higher densities give larger optical depths. Since the absorption coefficient in the Lyman continuum varies as ν^{-3} , an optical depth of 10 at 912Å corresponds to an optical depth of 1.6 at 500Å, a value sufficiently large to absorb most radiation at that wavelength.

Let us assume for simplicity that spicules are completely opaque to radiation in the wavelength interval 500-900Å. Consider a UV line formed in a transition region located below the tops of spicules. Near the center of the disk most of the UV radiation will be observed since spicules cover such a small fraction of the disk. However, near the limb where they cover a significant fraction of the disk, a substantial amount of the UV emission will be absorbed by foreground spicules if the wavelength of the UV line is to the blue side of the head of the Lyman continuum. If the wavelength is to the red side of the 912Å, the spicules will be transparent and no UV

radiation will be absorbed. Thus we would expect the limb brightening of optically thin lines to vary as $1/\mu$ if the wavelengths are longer than 912\AA , and vary less than $1/\mu$ for wavelengths shorter than 912\AA . This appears to be observed in the OSO-IV data.

The amount of light absorbed can be estimated if it is assumed that spicules are randomly distributed over the surface of the sun. It is well known that spicules are not randomly distributed, but assuming a random distribution provides a useful first order approximation. Let H_s be the height of the average spicule, W_s its width, and N_s the number of spicules per unit area. Let a UV line be formed in a geometrically thin transition region at a height H_t above the solar limb. Since the thickness of the transition region for $10^{4.6} \leq \tau_e \leq 10^{5.6}$ is less than 200 km, it is very thin compared to the typical height of spicules, 4000 to 6000 km.

Consider a circle with a radius ρR_\odot on the solar disk. As seen from the earth, all spicules on the solar surface that are within a distance $d = (H_s - H_t) \cdot \tan \theta$ will cross this circle (see Fig. 9). This means that all spicules within the band of length $2\pi\rho R_\odot$ and width d will cross the circle.

The number of spicules in the band is

$$N = 2\pi\rho R_{\odot} \cdot (H_s - H_t) \cdot \tan \theta \cdot N_s \quad (7)$$

Take the circumference $2\pi\rho R_{\odot}$ and divide into m lengths where $m = 2\pi\rho R_{\odot}/W_s$. The probability that an interval of length W_s will not be crossed by a spicule is given by the Poisson distribution:

$$\begin{aligned} P &= \exp(-N/m) \\ &= \exp\left[-N_s \cdot W_s \cdot (H_s - H_t) \cdot \tan \theta\right], \quad (8) \end{aligned}$$

Beckers' (1968) review paper gives for spicules

$$N_s = 3.3 \cdot 10^{-8} \text{ (km}^{-2}\text{)}$$

$$W_s = 825 \text{ km}$$

$$H_s = 4000 \text{ km}$$

$$H_t = 2000 \text{ km}$$

which gives

$$N_s \cdot W_s \cdot (H_s - H_t) = 0.05$$

Other H α features seen on the disk, which are either spicules or related to them, are the dark and the bright fine mottles.

For the dark mottles (Beckers, 1968),

$$N_s = 4.9 \cdot 10^{-8} \text{ (km}^{-2}\text{)}$$

$$W_s = 700 \text{ km}$$

$$H_s = 5000 \text{ km}$$

which gives

$$N_s \cdot W_s \cdot (H_s - H_t) = 0.10 .$$

For bright mottles

$$N_s = 1.3 \cdot 10^{-8} \text{ (km}^{-2}\text{)}$$

$$W_s = 3000 \text{ km}$$

$$H_s = 6500 \text{ km}$$

which gives

$$N_s \cdot W_s \cdot (H_s - H_t) = 0.18 .$$

These results suggest that for $H_t = 2000 \text{ km}$ the intensity of a UV line will vary as

$$I'(\rho) = I(\rho) \cdot e^{(-\sigma \cdot \tan \theta)}$$

where σ has a value between 0.05 and 0.2.

Figure 10 shows the limb brightening expected for an optically thin UV line formed in the transition region. The

wavelength is assumed to be shorter than 912\AA . The curves for several values of σ include the effects of the smoothing by the OSO-IV aperture function. They show that the absorption of UV radiation by spicules or other features observed from the ground in $H\alpha$ can significantly modify the character of limb brightening for UV lines with wavelengths capable of being absorbed in the Lyman continuum. The curves from Figure 10 have been plotted on the graphs giving limb brightening for lines $\lambda 765$ of N IV (Fig. 5), $\lambda 703$ of O III (Fig. 6), $\lambda 630$ of O V (Fig. 7), and $\lambda 554$ of O IV (Fig. 8). Table 2 gives the values of σ that best explain the limb brightening of these and several other lines with wavelengths less than 912\AA . The $\lambda 465$ line of Ne VII can be affected by spicular absorption in the He I continuum whose head is at 504\AA , as well as by absorption in the Lyman continuum. Note that the Ne VIII line at 770\AA and the Mg X line at 625\AA , which are formed respectively 1500 and 15000 km higher than the first 7 lines, are not appreciably affected by spicular absorption. In order to explain this result it is necessary to decrease σ by a factor of 3 to 4 when the height of line-formation is increased by approximately 1500 km. The exact dependence of σ on height depends critically on the distribution of spicules as a function of height. This distribution is

very poorly defined below heights of about 5000 km (cf. Becker, 1968). Analyses of spicular observations made at the limb indicate that the number of spicules reaching above a given height, $Q(h)$, decreases exponentially with increasing height. If all spicules have the same width, then $\sigma(h)$ will also vary exponentially with height. Figure 5 of Becker's (1968) review paper indicates that $Q(h)$ decreases by a factor of 1.3 to 5 between 2000 and 3500 km. The factor of 3 to 4 needed to explain UV observations falls within this range.

In principle one could determine the exact height of the transition region by using spicular statistics and limb brightening of UV lines formed at different heights. However, because the statistics contain substantial uncertainties, this is not possible. Given the limitations of these statistics and the simplified model used here, it appears to be quite reasonable to place the transition region at a height of about 2000 km above the visible surface of the sun.

5. Conclusions

This paper, together with Paper I, demonstrates that it is possible to explain limb brightening of a number of UV lines between 500-1400Å with a relatively simple model for

the transition region and lower corona, the modified Dupree-Goldberg model described in Section 3. The present paper also demonstrates the importance of introducing into the simple stratified coronal model the effects of spicules that penetrate into the transition region. If spicules are optically thick in the Lyman continuum at wavelengths between 500 and 900Å, constraints are placed on the range of temperature and densities allowable in spicules.

ACKNOWLEDGEMENTS

I am indebted to Dr. L. Goldberg, Dr. R.W. Noyes, Dr. W. H. Parkinson, and Dr. E.M. Reeves who contributed so much time and effort to making the Harvard OSO-IV experiment a success. I am grateful to them and Dr. A.K. Dupree for many stimulating discussions on the significance of different aspects of the OSO-IV observations. This work was supported by the National Aeronautics and Space Administration through contract NASw-184.

References

- ATHAY, R.G.: 1966, Astrophys. J. 145, 784.
- BECKERS, J.M.: 1968, Solar Phys. 3, 367.
- DUPREE, A.K. and GOLDBERG, L.: 1967, Solar Phys. 1, 229.
- GIOVANELLI, R.G.: 1967, Aust. J. Phys. 20, 81.
- PURCELL, J.D. and TOUSEY, R.: 1969, Special Meeting on Solar Astronomy of American Astronomical Society, Pasadena, California.
- WITHBROE, G.L.: 1969, submitted for publication.

TABLE 1

The Optical Thickness of the Line-Forming
Region for a Number of XUV Lines

λ (Å)	Ion	τ	No. Orbits Used	T_{\max} (K)
1394	Si IV	0.30	1	0.8×10^5
1238	N V	0.04	1	2.0×10^5
1032	O VI	0.27	7	3.3×10^5
991	N III	0.07	5	1.0×10^5
977	C III	1.24	4	0.9×10^5
770	Ne VIII	0.05	6	7.1×10^5
765	N IV	0.03	2	1.6×10^5
703	O III	0.07	4	1.1×10^5
630	O V	0.15	3	2.6×10^5
625	Mg X	0.14	5	1.3×10^6
554	O IV	0.06	3	2.0×10^5
499	Si XII	0.18	7	2.5×10^6

T_{\max} is the temperature at which formation of the ion is most strongly favored.

TABLE 2

Spicular Cross Sections, σ ,
Necessary for Different Lines

λ (Å)	Ion	σ (see text)
765	N IV	0.15
758	O V	0.2
703	O III	0.2
630	O V	0.18
600	O III	0.15
554	O IV	0.13
465	Ne VII	0.1
770	Ne VIII	0.05
625	Mg X	0.0

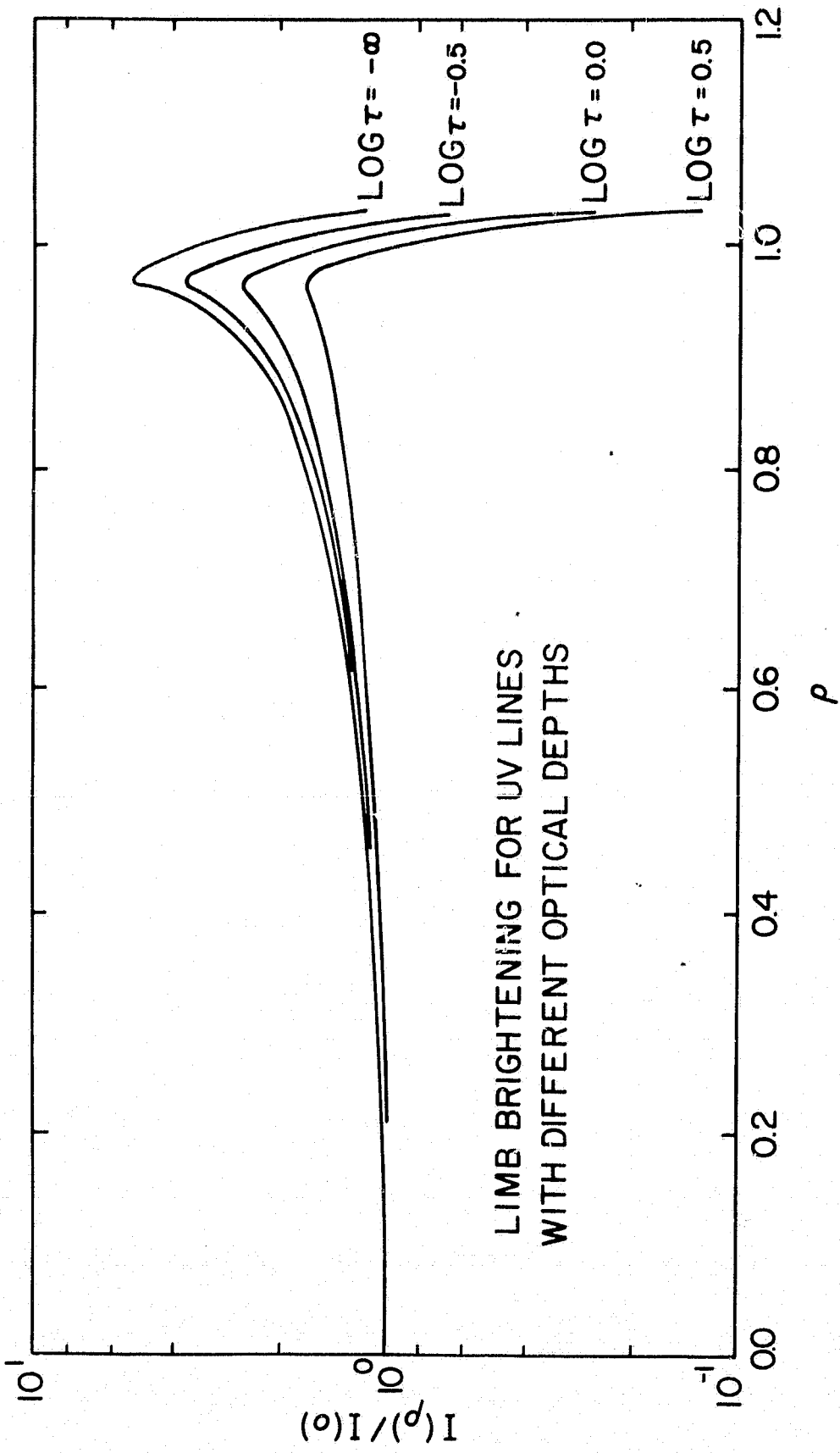


FIG. 1

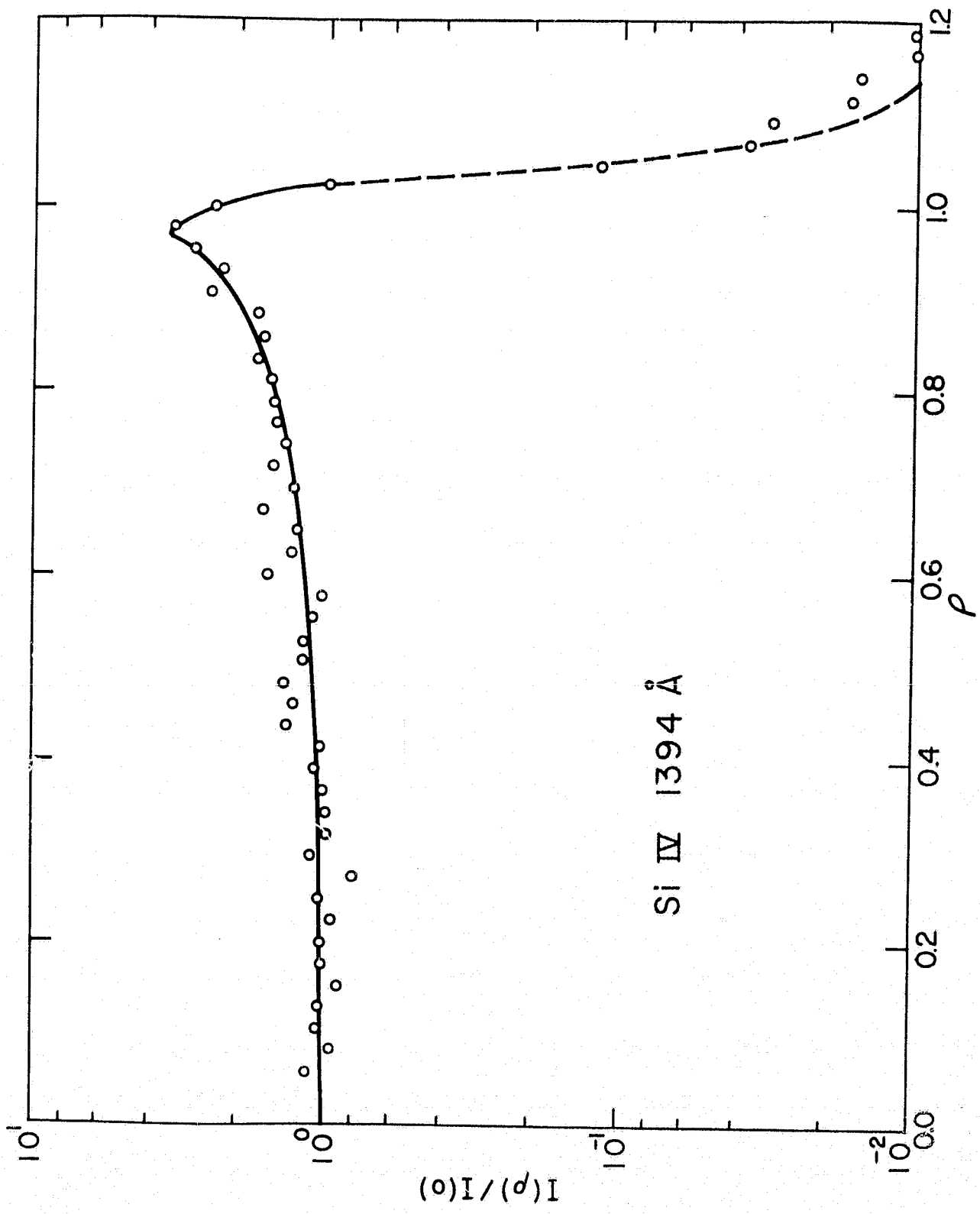


FIG. 2

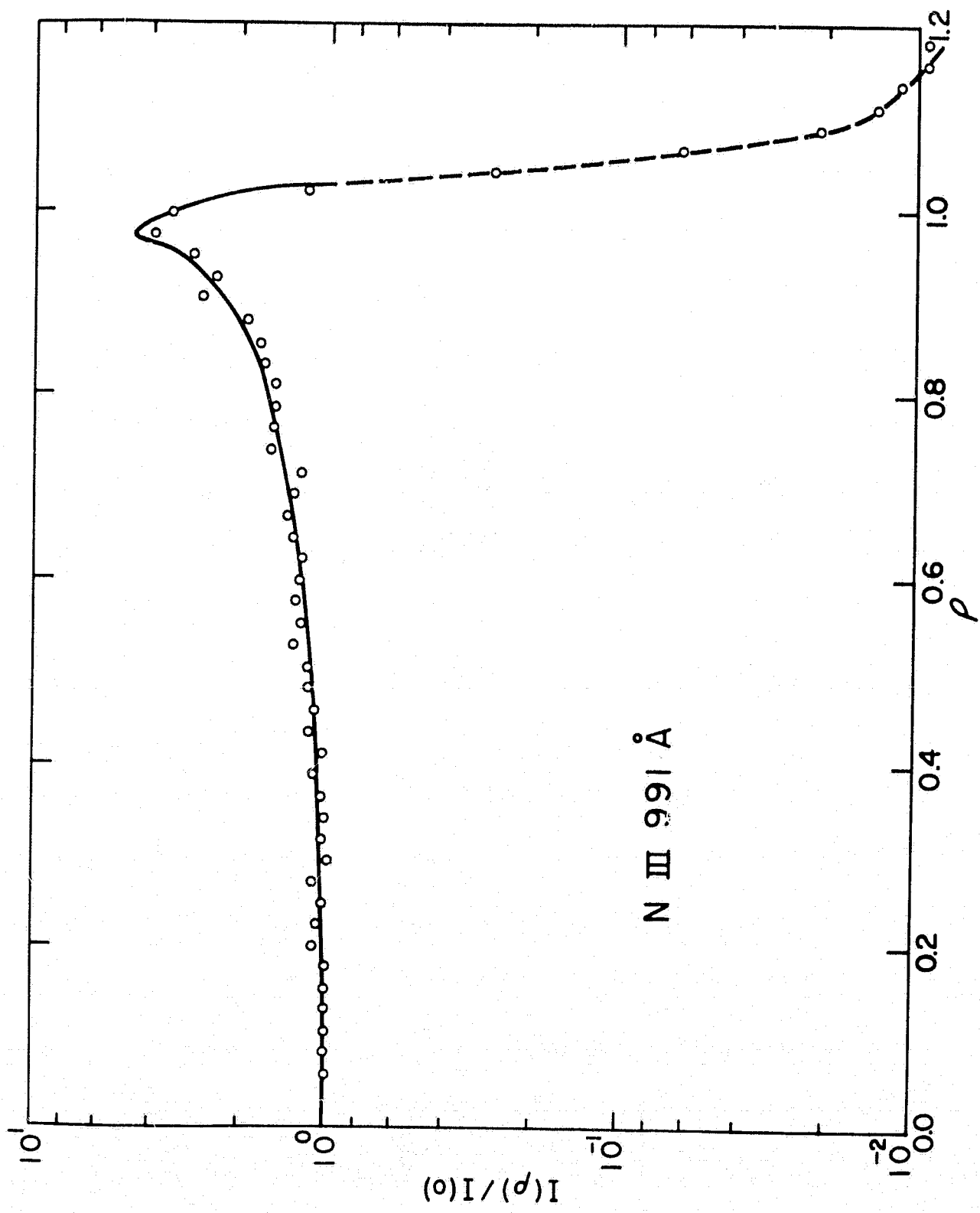


FIG. 3

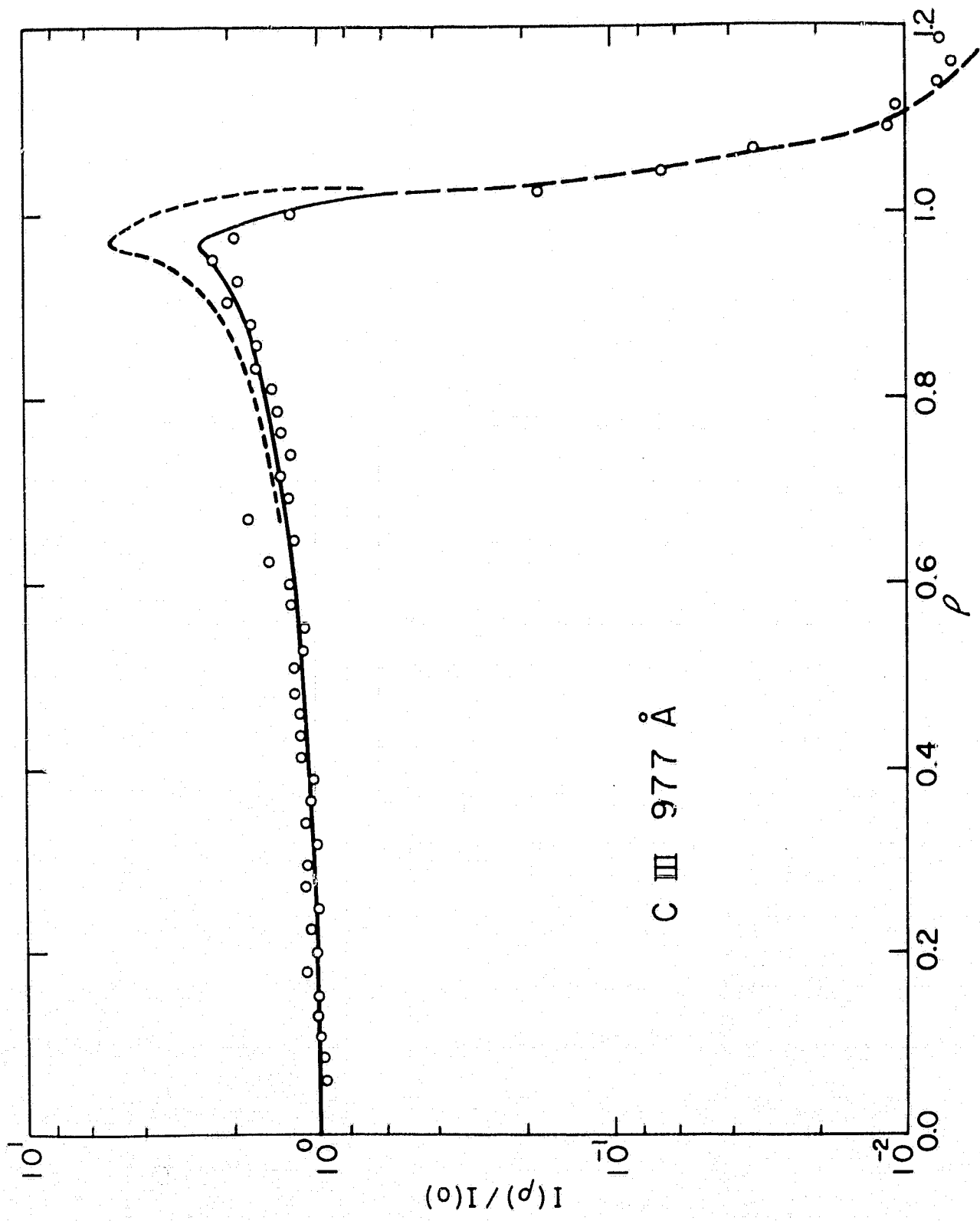


FIG. 4

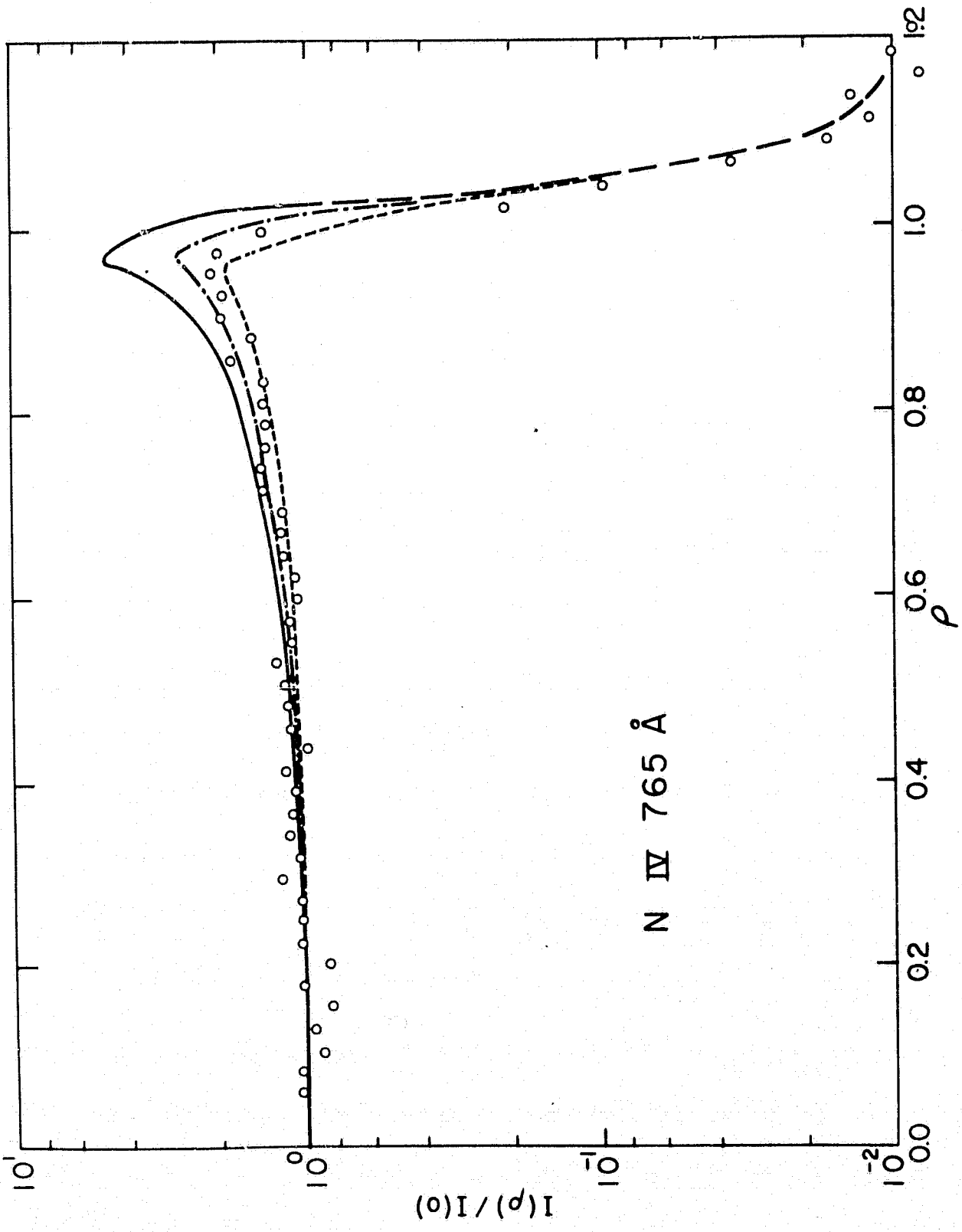


FIG. 5

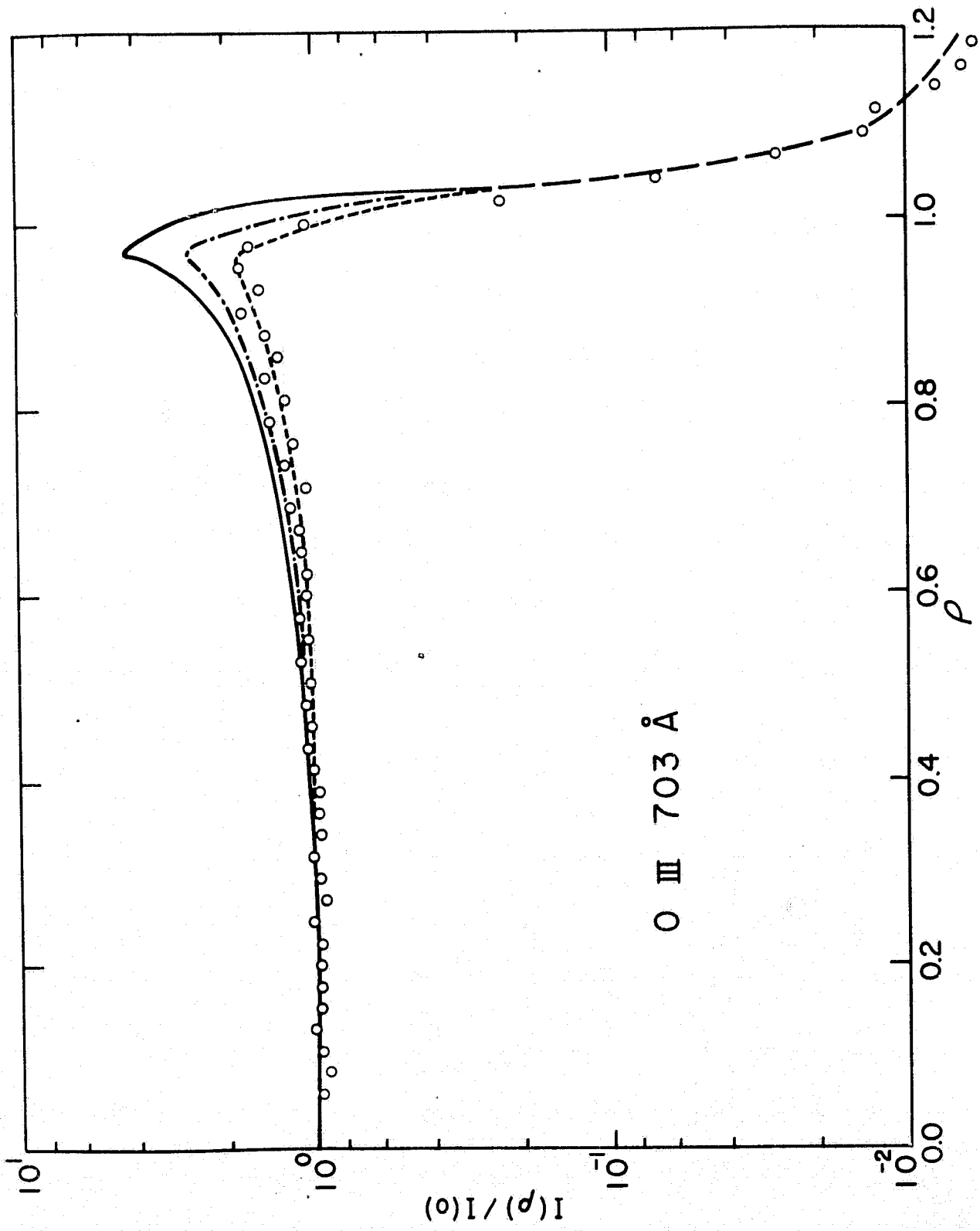


FIG. 6

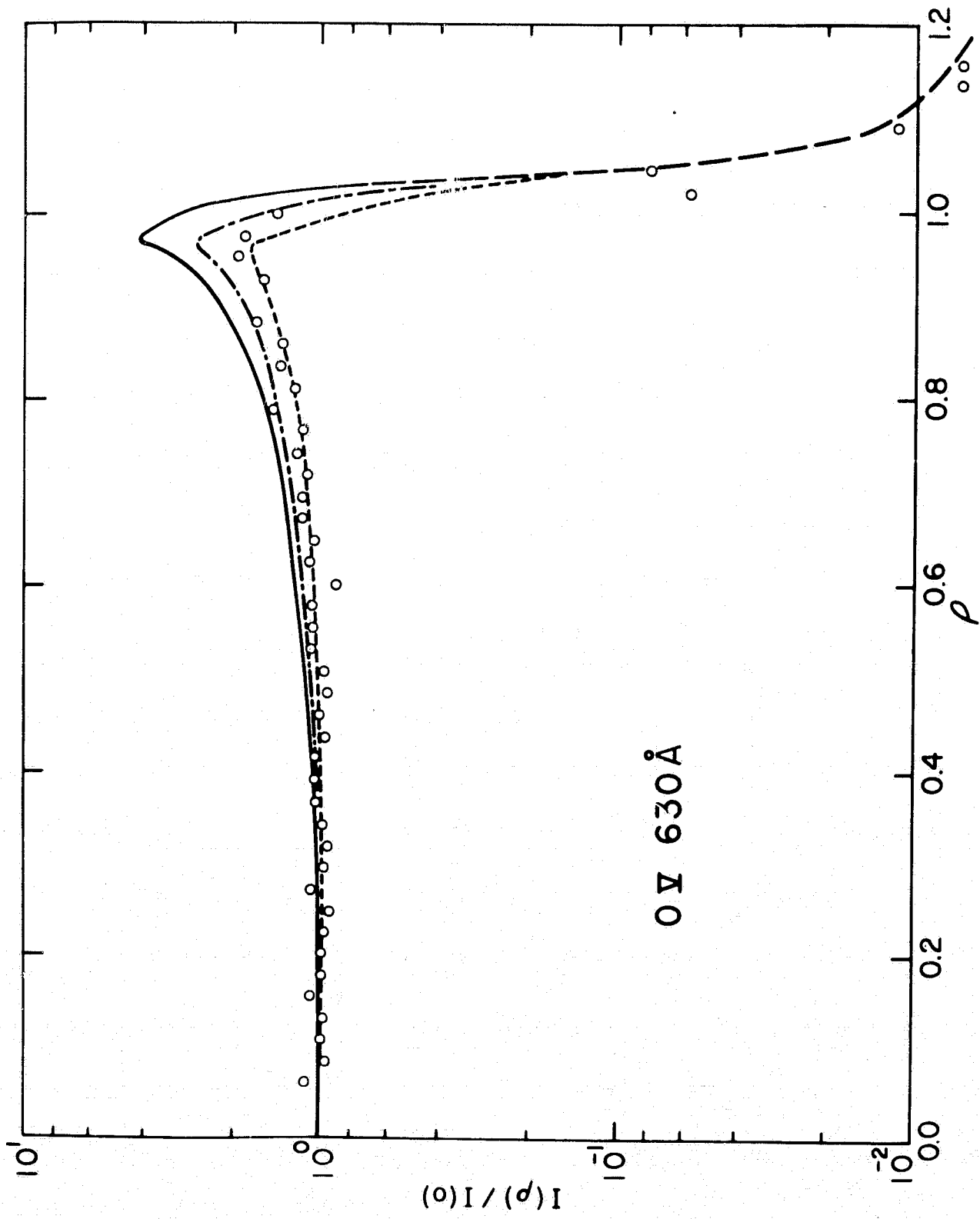


FIG. 7

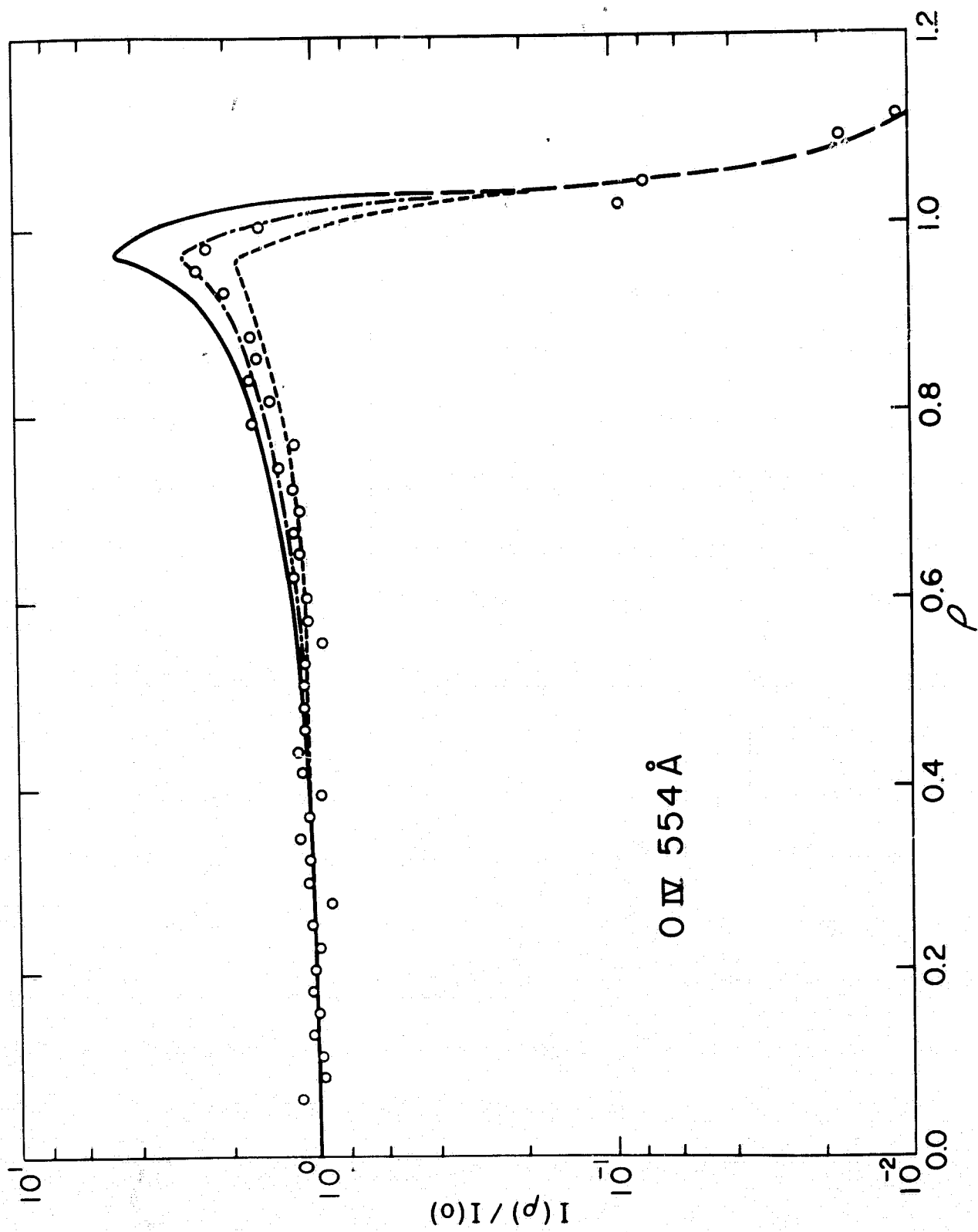


FIG. 8

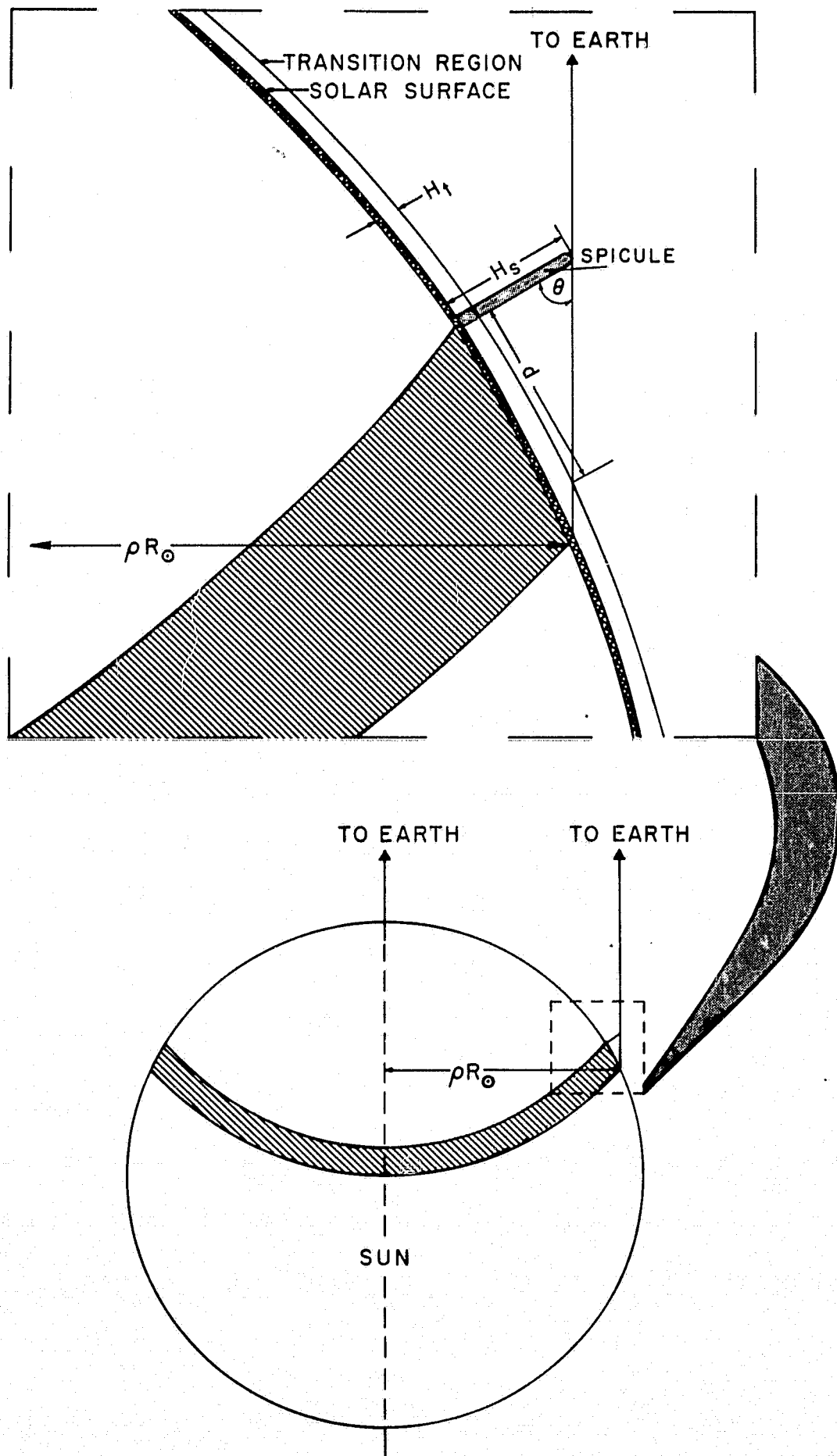


FIG. 9

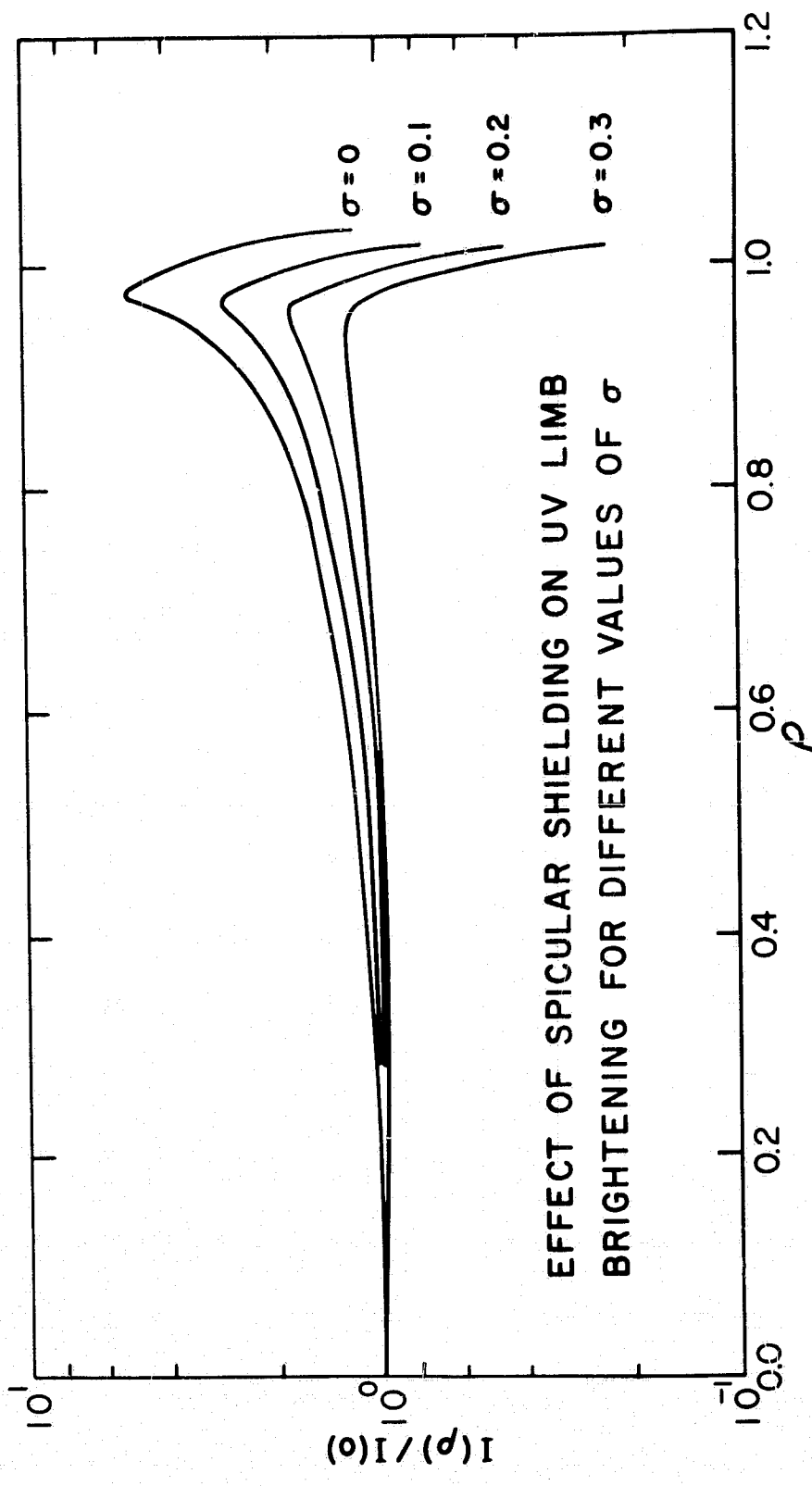


FIG. 10.

Figure Captions

- Figure 1. The center-to-limb variation of the intensity of XUV emission lines with different optical depths τ .
- Figure 2. The center-to-limb variation of the intensity of the Si IV line at $\lambda 1394$. The points represent the mean of the observed intensities at a given value of ρ averaged over the range $\rho \pm 0.012$. The solid line is the variation predicted by the modified Dupree and Goldberg model. The dashed line for $\rho > 1$ is the mean limb profile determined from spectroheliograms in many low excitation lines.
- Figure 3. The center-to-limb variation of the intensity at $\lambda 991$ of N III.
- Figure 4. The center-to-limb variation of the intensity at $\lambda 977$ of C III. The solid line is the limb brightening predicted by the model. The C III line has an optical depth of approximately unity. For comparison, the dotted line shows the limb brightening for an optically thin line.
- Figure 5. The center-to-limb variation of the intensity at $\lambda 765$ of N IV. The solid line is the limb brightening predicted by the modified Dupree and Goldberg model. The dot-dashed line shows the

effect of introducing spicular shielding for $\sigma = 0.1$ (see text). The lower dashed line is for $\sigma = 0.2$.

- Figure 6. Same as Figure 5, but for $\lambda 703$ of O III.
- Figure 7. Same as Figure 5, but for $\lambda 630$ of O V.
- Figure 8. Same as Figure 5, but for $\lambda 554$ of O IV.
- Figure 9. Geometry used in defining equation 8 (see text).
- Figure 10. The effect of spicular shielding on the center-to-limb variation of the intensity of an XUV line formed below the tops of spicules. The upper curve is the limb brightening for an optically thin line. The other curves show the effect of spicular shielding for different values of σ .